doi:10.1093/brain/awv081 BRAIN 2015: 138; 1738–1755 | 1738

BRAIN
A JOURNAL OF NEUROLOGY

Reactive microglia drive tau pathology and contribute to the spreading of pathological tau in the brain

Nicole Maphis,[1] Guixiang Xu,[2] Olga N. Kokiko-Cochran,[2] Shanya Jiang,[1] Astrid Cardona,[3] Richard M. Ransohoff,[4] Bruce T. Lamb[2] and Kiran Bhaskar[1]

Pathological aggregation of tau is a hallmark of Alzheimer's disease and related tauopathies. We have previously shown that the deficiency of the microglial fractalkine receptor (CX3CR1) led to the acceleration of tau pathology and memory impairment in an hTau mouse model of tauopathy. Here, we show that microglia drive tau pathology in a cell-autonomous manner. First, tau hyperphosphorylation and aggregation occur as early as 2 months of age in hTau*Cx3cr1*$^{-/-}$ mice. Second, CD45^{+} microglial activation correlates with the spatial memory deficit and spread of tau pathology in the anatomically connected regions of the hippocampus. Third, adoptive transfer of purified microglia derived from hTau*Cx3cr1*$^{-/-}$ mice induces tau hyperphosphorylation within the brains of non-transgenic recipient mice. Finally, inclusion of interleukin 1 receptor antagonist (Kineret®) in the adoptive transfer inoculum significantly reduces microglia-induced tau pathology. Together, our results suggest that reactive microglia are sufficient to drive tau pathology and correlate with the spread of pathological tau in the brain.

1 Department of Molecular Genetics and Microbiology, MSC08 4660, 1 University of New Mexico, University of New Mexico, Albuquerque NM 87131, USA
2 Department of Neurosciences, NC30, 9500 Euclid Avenue, Cleveland Clinic, Cleveland OH 44195, USA
3 Department of Biology, University of Texas San Antonio, West Campus/Tobin lab MBT 1.216, San Antonio TX 78249, USA
4 Biogen Idec, 225 Binney Street, Cambridge, MA 02142, USA

Correspondence to: Kiran Bhaskar,
Department of Molecular Genetics and Microbiology MSC08 4660,
1 University of New Mexico, University of New Mexico,
Albuquerque NM 87131,
USA
E-mail: KBhaskar@salud.unm.edu; KBhaskar@unm.edu

Keywords: Alzheimer's disease; tauopathies; tau protein; microglia; neuroinflammation

Abbreviations: IL-1Ra = interleukin-1 receptor antagonist; p38 MAPK = p38 mitogen activated protein kinase

Introduction

The hyperphosphorylation and aggregation of microtubule-associated protein tau (MAPT) forms the initial aetiological insult prior to neurodegeneration in tauopathies, which include progressive supranuclear palsy, corticobasal degeneration, Alzheimer's disease and many others (Lee *et al.*, 2001). Recent studies have suggested that misfolded tau can affect neuronal integrity via several mechanisms including microtubule instability, defective axonal transport, synaptic deficits, exacerbating amyloid-β-mediated pathologies as well as trans-synaptic spreading within anatomically connected brain regions (Morris *et al.*, 2011; Bhaskar, 2012; Liu *et al.*, 2012). However, the mechanisms leading

Received August 29, 2014. Revised January 6, 2015. Accepted January 27, 2015. Advance Access publication April 1, 2015

to elevated tau hyperphosphorylation and aggregation still remain unclear. Neuroinflammation, which positively correlates with tau pathology, has been implicated in driving tau hyperphosphorylation, aggregation and neurodegeneration in various human (Gebicke-Haerter, 2001; Ishizawa and Dickson, 2001; Gerhard *et al.*, 2006; Bellucci *et al.*, 2011) and rodent models of tauopathies (Bellucci *et al.*, 2004; Ikeda *et al.*, 2005; Yoshiyama *et al.*, 2007; Sasaki *et al.*, 2008; Zilka *et al.*, 2009). First, activated microglia are found to spatially co-exist with tau-burdened neurons in the brains of patients with progressive supranuclear palsy and corticobasal degeneration (Ishizawa and Dickson, 2001; Gerhard *et al.*, 2004, 2006). Second, microglial activation has been demonstrated to precede tau pathology in the P301S mouse model of tauopathy (Yoshiyama *et al.*, 2007). Notably, administration of an immunosuppressant drug (FK506) attenuated microglial activation and extended the life span of P301S mice (Yoshiyama *et al.*, 2007). Third, induction of systemic inflammation via administration of the toll-like receptor 4 (TLR4) ligand, lipopolysaccharide, significantly induced tau hyperphosphorylation in a triple transgenic mouse model of Alzheimer's disease (Kitazawa *et al.*, 2005). Subsequent studies from this group have suggested that the blocking or sustained activation of interleukin 1 (IL1) signalling leads to attenuation or exacerbation of tau pathology, respectively (Kitazawa *et al.*, 2011). While these studies suggested that inflammatory alterations might induce tau pathology and neurodegeneration, there is little mechanistic evidence for the role of microglia in this process.

We have previously provided compelling evidence that chemically or genetically enhancing microglial activation significantly accelerated tau pathology and behavioural abnormalities in the hTau mouse model of tauopathy (Bhaskar *et al.*, 2010). Deficiency of microglia-specific fractalkine receptor (CX3CR1) in hTau mice resulted in elevated microglial activation, accelerated tau pathology as well as impaired working memory (Bhaskar *et al.*, 2010). Additional mechanistic studies suggested that this effect is mediated via activation of the neuronal IL-1 receptor (IL-1R)-p38 mitogen activated protein kinase (p38 MAPK) signalling pathway. Such effects of *Cx3cr1* deficiency on tau pathology have also been observed in other (hAPP) models of neurodegeneration (Cho *et al.*, 2011). These studies suggest that microglia-specific neuroinflammation accelerates tau pathology and leads to neurodegeneration. However, it is still unclear whether reactive microglia themselves are sufficient to drive neuronal tau phosphorylation/aggregation and eventually lead to the spread of tau pathology.

In the current study, we first evaluated the onset and progression of tau pathology as a function of CX3CR1 deficiency in hTau mice at different disease stages. Next, we assessed the spatio-temporal correlation between the spread of tau hyperphosphorylation and $CD45^+$ microglia in anatomically connected regions of the hippocampus of hTau*Cx3cr1*$^{-/-}$ mice. We then examined spatial memory in hTau*Cx3cr1*$^{-/-}$ mice to determine if microglial activation and tau pathology correlates with functional deficits. Finally, we performed adoptive transfer of purified microglia derived from hTau*Cx3cr1*$^{-/-}$ mice to determine whether reactive microglia are sufficient and directly induce tau pathology within the brains of naïve non-transgenic recipient mice.

Materials and methods

Mice

The hTau (Andorfer *et al.*, 2003) (expressing human *MAPT* and deficient for endogenous mouse *Mapt*) and *Cx3cr1*$^{-/-}$ (Jung *et al.*, 2000) [targeted deletion of *Cx3cr1* via insertion of green fluorescence protein (GFP) gene into the *Cx3cr1* locus] mice were crossed and maintained in the C57BL/6J genetic background and were obtained from the Jackson Laboratory and Dan Littman (HHMI, New York University School of Medicine). The hTau*Cx3cr1*$^{-/-}$ mice were generated as previously described (Bhaskar *et al.*, 2010). All experimental protocols involving animals were performed in accordance with US National Institutes of Health guidelines on animal care and were approved by the University of New Mexico and Cleveland Clinic Institutional Animal Care and Use Committees.

Antibodies and reagents

MAPT antibodies: mouse monoclonal antibodies AT8, AT180 (Pierce) and Tau5 (Invitrogen); PHF-1 (provided by Peter Davies, Albert Einstein College of Medicine). Inflammatory markers: rabbit polyclonal antibody against ionized calcium binding adaptor molecule 1 (Iba1) (Wako), rat monoclonal antibodies against CD68 and CD45 (Serotec). Other antibodies: mouse monoclonal antibody against GAPDH; mouse monoclonal NeuN (Millipore), total p38 MAPK and activated p38 MAPK (phospho-T180/Y182) (Cell Signaling for western blotting; Invitrogen for Immunohistochemistry); mouse monoclonal antibody against SNAP25 (a kind gift from the late Dr Michael Wilson, University of New Mexico). Other reagents: interleukin-1 receptor antagonist (IL-1Ra) (Kineret®, Amgen).

Tissue preparation and measurement of hippocampal wet weight

Prior to biochemical and neuropathological analysis, the mice were anaesthetized and transcardially perfused with phosphate buffer and the brains were removed. The left hemisphere was immerse fixed in 4% paraformaldehyde and the hippocampi from the right hemisphere were micro-dissected and the wet weights were recorded before freezing in liquid nitrogen for subsequent biochemical analysis.

SDS-PAGE and western immunoblotting

Proteins were homogenized in the Tissue Protein Extraction Reagent (TPER®, Thermo Scientific) and soluble hippocampal lysates were resolved via SDS-PAGE and immunoblotted as

previously described (Bhaskar *et al.*, 2010). The dilutions of primary antibodies used were as follows: AT8 1:5000; AT180 1:2500; PHF-1 1:5000; Tau5 1:5000; GAPDH 1:10 000; phospho-p38 MAPK and total p38 MAPK 1:1000; SNAP25 1:2500. See the online Supplementary material for additional details on SDS-PAGE/western blotting.

Immunohistochemistry, quantitative morphometry and Gallyas silver staining

Free-floating random sections (30 µm thick) derived from multiple mouse brains per group were utilized for all of the immunohistochemical and immunofluorescence analysis. The antibody dilutions were: AT8, AT180, NeuN, p-p38 MAPK (T180/Y182) and CD45 at 1:250; Iba1 at 1:500 incubated overnight at 4°C. Secondary antibodies (1:250) conjugated to either biotin (for immunohistochemistry from Vector Laboratories) or Alexa Fluor® dyes (for immunofluorescence from Life Technologies) were used. Sections were then either mounted in DAPI Hardset Reagent (for immunofluorescence) or incubated with Avidin/Biotinylated enzyme Complex (ABC reagent, Vector Laboratories; for immunohistochemistry) reagent for 1 h at room temperature. The immunoreactive signals were revealed by developing sections in SigmaFast® 3,3′-diaminobenzidine (DAB) either with (Sigma*Fast*® DAB with $CoCl_2$ metal enhancer) or without metal enhancer and urea tablets (Sigma-Aldrich). Bright field and epifluorescence images were acquired using Leica DMR upright fluorescence/bright field microscope. Confocal images were acquired and analysed with Leica TCS-SP and SP-AOBS upright confocal microscopes with Leica confocal software or a Zeiss inverted Meta confocal machine and composed the images and videos via Zeiss Zen software.

For the quantitative morphometry, NIH ImageJ was used to quantify the percentage of CD45 and p-p38 MAPK immunoreactive areas. The number of $AT180^+$ and $NeuN^+$ neurons, AT8 immunoreactivity and $EGFP^+$ microglia in the adoptive transfer experiments were manually scored in four random sections/mouse. See the Supplementary material for additional details on immunohistochemical analysis and quantitative morphometry. The Gallyas silver staining on 30 µm free-floating sections was performed as described (Braak and Braak, 1991; Bhaskar *et al.*, 2010).

Morris Water Maze

The mice were tested in the visible (for 3 days) and hidden (for 4 days) platform task of the Morris Water Maze (Morris, 1984). See Supplementary material for a detailed description.

Isolation and adoptive transfer of microglial cells

Mononuclear cells were isolated from a pool of two brains per group as previously described (Bergmann *et al.*, 1999) (Fig. 5C). Briefly, the mice were anaesthetized, transcardially perfused with phosphate buffer, brains removed and dissociated in 0.25% trypsin/RPMI media. Mononuclear cells were separated via a 30%/70% discontinuous isotonic Percoll® gradient followed by magnetic assisted cell sorting (Dynabead FlowComp™ Flexi kit, Cat # 110-61D; Life Technologies; DSB-X™ Biotin Protein Labeling Kit, Life Technologies; Cat # D-20655) using the CD11b antibody (Millipore) and elution method as per the manufacturer's protocol. Purified microglia (0.5×10^5 cells/ml, in 50 µl) from donor mice with described genotypes or vehicle (RPMI media) were injected with or without IL-1Ra (Kineret®, Amgen; 3 ng) into the brains of 2-month-old C57BL/6J non-transgenic recipient mice with the following stereotaxic co-ordinates: from Bregma: −1.94 mm posterior; 1.5 mm lateral; 1.5 mm dorsoventral, as previously described by Cardona *et al.* (2006). After 72 h, the recipient mice were perfused with 4% paraformaldehyde and the brains were processed for immunofluorescence analysis for AT8 and GFP^+ microglia and quantitative morphometry as described in the Supplementary material.

Gene expression analysis

RNA from the hemi-brain was extracted using TRI Reagent® Solution as described by the manufacturer (Invitrogen). Total RNA (50 ng/µl) was converted to cDNA using the High Capacity cDNA Reverse Transcription kit (Applied Biosystems Inc., ABI) and amplified using specific TaqMan® probes [for CD45 (now known as *Ptprc*) and *Il1B*] and *Gadph* was used as a housekeeping gene for normalization, on the StepOnePlus® Real-Time PCR System (Life Technologies).

Sarkosyl insoluble assay

The Sarkosyl-insoluble fraction of MAPT was isolated from hippocampal tissues as described previously (Greenberg and Davies, 1990) with minor modifications, which have been previously described (Bhaskar *et al.*, 2010).

Primary microglial culture

Microglial cultures were prepared from post-natal Day 3 (P3) pups from $Cx3cr1^{+/-}$ or $Cx3cr1^{-/-}$genotypes as previously described (Saura *et al.*, 2003; Bhaskar *et al.*, 2010). See Supplementary material for a description of the primary microglial culture.

IL1B assay in HEK-Blue™ reporter cells

HEK-Blue™ IL1B cells (InvivoGen) specifically respond to IL1B. Once IL1B binds to its receptor IL-1R on the surface of HEK-Blue™ IL1B cells, this triggers a signalling cascade leading to the activation NF-κB and the subsequent production of secreted embryonic alkaline phosphatase (SEAP). Induced SEAP levels in the supernatant of HEK-Blue™ IL1B cells can be assessed using QUANTI-Blue™, a SEAP detection medium. QUANTI-Blue™ turns blue in the presence of SEAP (Fig. 4C), which can be easily quantified using a spectrophotometer. The intensity of the colour reaction is proportional to the amount of IL1B in the supernatant from hippocampal lysates measured. IL1B levels in the samples

can be determined by making a standard curve using standards (recombinant murine IL1B).

Hippocampal lysates were prepared by homogenizing in tissue-protein extraction reagent (T-PER, 78510; Pierce) with protease (p8340; Sigma-Aldrich) and phosphatase (p5726; Sigma-Aldrich) inhibitor cocktails. Lysates were spun down and the supernatant was saved. Supernatant (50 µl) and different concentrations of standards (recombinant murine IL1B) were then transferred onto 150 µl (~50 000 cells) of HEK-Blue™ IL1B reporter cells (InvivoGen), which respond to mouse IL1B by expressing a reporter gene (SEAP). HEK-Blue™ IL1B reporter cells were incubated overnight and the supernatant of HEK-Blue™ IL1B reporter cells was then incubated with QUANTI-Blue™ for 1 h at 37°C. Induced SEAP levels were measured by spectrophotometry at 620 nm. The intensity of the colour reaction is proportional to the amount of IL1B in the supernatant from hippocampal lysates. IL1B levels in the supernatant were determined by the standard curve.

Results

Deficiency of *Cx3cr1* in hTau mice lead to epitope-specific tau hyperphosphorylation and aggregation at 2 months of age

We performed an age-based study to determine how early tau pathology begins and how it progresses at different stages of disease in hTau*Cx3cr1*$^{-/-}$ mice. Two groups of mice were analysed: (i) hTau mice (Andorfer *et al.*, 2003), which are deficient for endogenous mouse tau and express all six isoforms of non-mutant human tau; and (ii) hTau mice lacking the microglial receptor, CX3CR1 (hTau*Cx3cr1*$^{-/-}$ mice). Separate groups of mice were aged to 2, 6, 12 or 24 months and the hippocampi were processed for western blot and immunohistochemical analysis to determine tau phosphorylation and activation of p38 MAPK.

Tau phosphorylation on the AT8 (pS202), AT180 (pT231) and PHF-1 (pS396/S404) sites were elevated in hTau*Cx3cr1*$^{-/-}$ mice as early as 2 months of age compared to hTau mice. Consistent with our prior observations (Bhaskar *et al.*, 2010), 6-month-old hTau*Cx3cr1*$^{-/-}$ mice showed elevated levels of tau phosphorylated at AT8, AT180 and PHF-1 sites (Fig. 1A) compared to other groups. Upon quantification, we observed AT8-, AT180- and PHF-1-site tau phosphorylation was significantly higher in hTau*Cx3cr1*$^{-/-}$ mice compared to hTau at 2- and 6-months of age (Fig. 1B–D). By 12 months of age, the hTau mice showed AT8 and PHF-1 site tau phosphorylation that were indistinguishable from that of hTau*Cx3cr1*$^{-/-}$ mice (Fig. 1A–D). Interestingly, there was an overall reduction in AT8, AT180 and PHF-1 site phosphorylation at older age groups of both genotypes compared to younger groups.

In a previous study, we identified significantly increased activation of p38 MAPK in hTau*Cx3cr1*$^{-/-}$ mice at 6 months of age (Bhaskar *et al.*, 2010). A biphasic response was observed for active p38 MAPK (phosphorylated at T180/Y182) in the hippocampus of hTau and hTau*Cx3cr1*$^{-/-}$ mice (Fig. 1E). Notably, active p38 MAPK was already present in 2-month-old hTau and hTau*Cx3cr1*$^{-/-}$ mice. The level of active p38 MAPK was significantly reduced to undetectable levels in hTau mice at 6 months of age, but remained elevated in hTau*Cx3cr1*$^{-/-}$ mice (Fig. 1A and E). At later stages (12- and 24-months of age), a modest but stable increase in the level of phospho-p38 MAPK was observed in hTau mice (Fig. 1A and E). Unlike p38 MAPK, we did not detect any significant alterations in the levels of activated ERK/JNK kinases across ages or between the two groups.

Consistent with the biochemical studies, immunohistochemical analysis revealed the presence of AT8^{+} neurons in the dentate gyrus of hTau mice at 6 months of age and continued to exist until 24 months of age, but with a small dip at 12 months (Fig. 2A and C). A significant increase in the AT8^{+} cells in the hilus of the dentate gyrus in hTau*Cx3cr1*$^{-/-}$ mice was apparent as early as 2 months of age (Fig. 2A and C) and stayed elevated through to 24 months of age (Fig. 2A). A similar pattern of immunoreactivity was also observed for AT180 (Fig. 2B) with elevation of AT180 positive neurons in the hilus of dentate gyrus in 2-month-old hTau*Cx3cr1*$^{-/-}$ mice compared to hTau mice (Fig. 2B and 2C; lower magnification images are in Supplementary Fig. 2). Notably, the CA3 region of the hippocampus also displayed a similar increase in AT8 and AT180 immunoreactive neurons in hTau*Cx3cr1*$^{-/-}$ mice as early 2 months of age (Supplementary Fig. 1A and B). Overall, we observed a consistent immunoreactive pattern between biochemical (western blot) and immunohistochemical analysis for AT8 and AT180. For example, there was a small drop in the overall AT8/AT180 immunoreactive area at older ages compared to younger groups (Fig. 2C). However, correlating the tau immunoreactivity in different subregions of the hippocampus (dentate gyrus and CA3) with those observed in the entire hippocampus via western blot analysis suggest subregion-specific variability in tau phosphorylation in hTau and hTau*Cx3cr1*$^{-/-}$ mice with increasing age.

To determine whether 2-month-old hTau*Cx3cr1*$^{-/-}$ mice display any signs of pathological aggregation of tau, we performed Gallyas silver staining—a standard method for the detection of aggregated tau, pre- and mature tangles (Braak and Braak, 1991). In comparison to our previous study where we observed silver positive mature tangles in 6-month-old hTau*Cx3cr1*$^{-/-}$ mice (Bhaskar *et al.*, 2010), a majority of the neurons in the CA1 region (Fig. 2D) displayed granules of silver aggregates within their cell bodies in 2-month-old hTau*Cx3cr1*$^{-/-}$, but not in age-matched hTau mice (Fig. 2D). No silver positive granulations were observed in 2-month-old non-transgenic and *Cx3cr1*$^{-/-}$ mice (data not shown). To confirm the pre-tangle

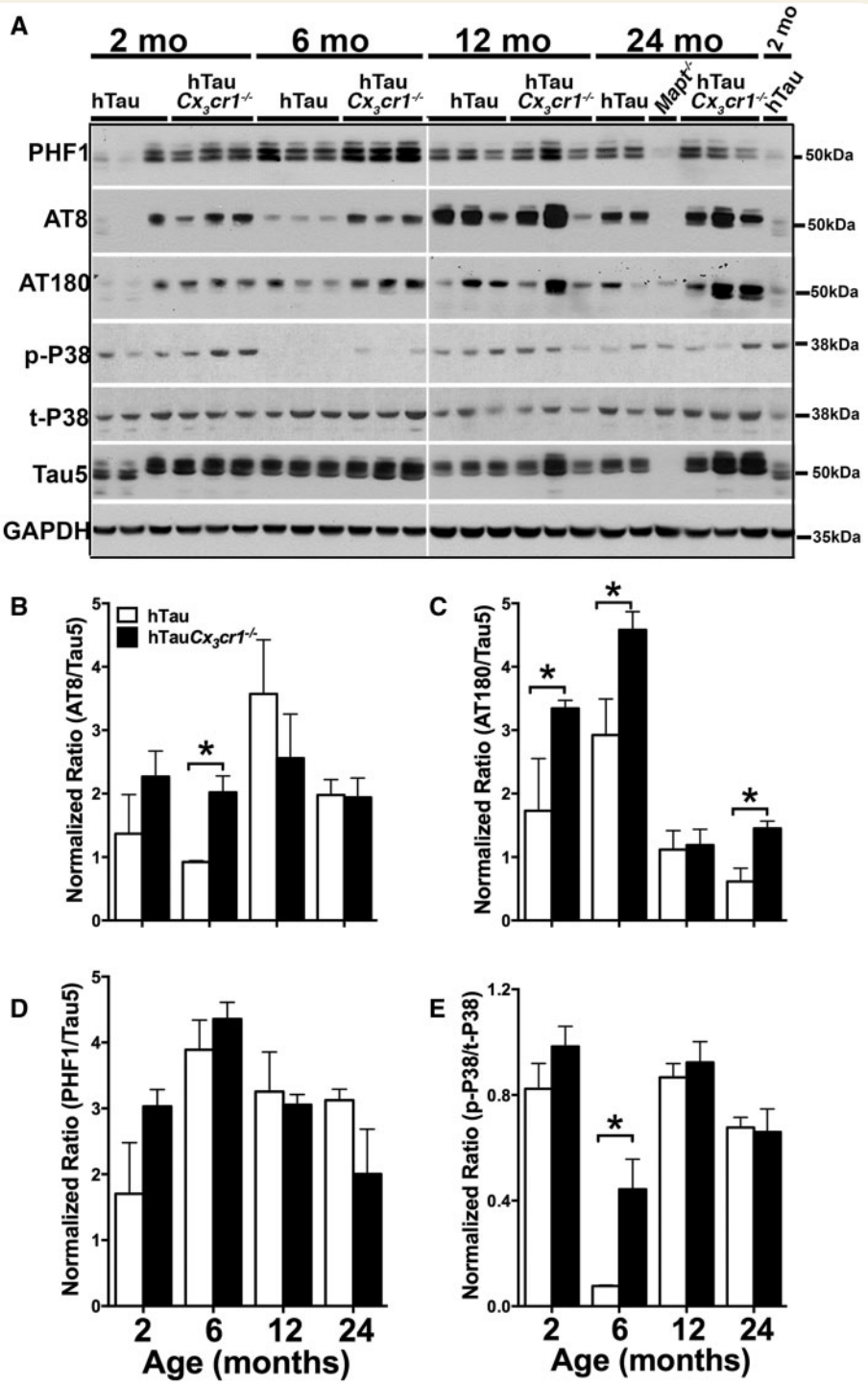

Figure 1 CX3CR1 deficiency accelerates tau hyperphosphorylation and p38 MAPK activation in hTau mice at early stages of development. (**A**) Western blot analysis of hippocampal lysates shows elevated tau phosphorylation on AT8, AT180 and PHF-1 sites and activation of p38 MAPK (pT180/pY182) in hTau*Cx3cr1*$^{-/-}$mice at 2 months of age. No significant alterations in total tau (Tau5 antibody) or total (t) p38 MAPK levels. GAPDH was the loading control. Lysates from tau knockout mice were included in the *Mapt*$^{-/-}$ lane and show no expression of tau. (**B–E**) Quantification of western blots for AT8, AT180, PHF-1 and phospho (p)-p38 MAPK reveal a statistically significant [$n = 5$ per group for 2, 12 and 24-month-old groups; $n = 6$ for 6-month-old group; mean ± SEM integrated density value ratio for respective epitopes (*$P < 0.05$ and **$P < 0.01$; two-way ANOVA Bonferroni's multiple comparisons test)] increase in AT8 (**B**), AT180 (**C**), PHF-1 (**D**) and p-p38 MAPK (**E**) at 2-, 6- and/or 24-months of age in hTau*Cx3cr1*$^{-/-}$mice compared to hTau mice. For p-p38 MAPK, both hTau and hTau*Cx3cr1*$^{-/-}$mice show a biphasic response (overall increase at 2-, 12- and 24-months, reduction at 6 months).

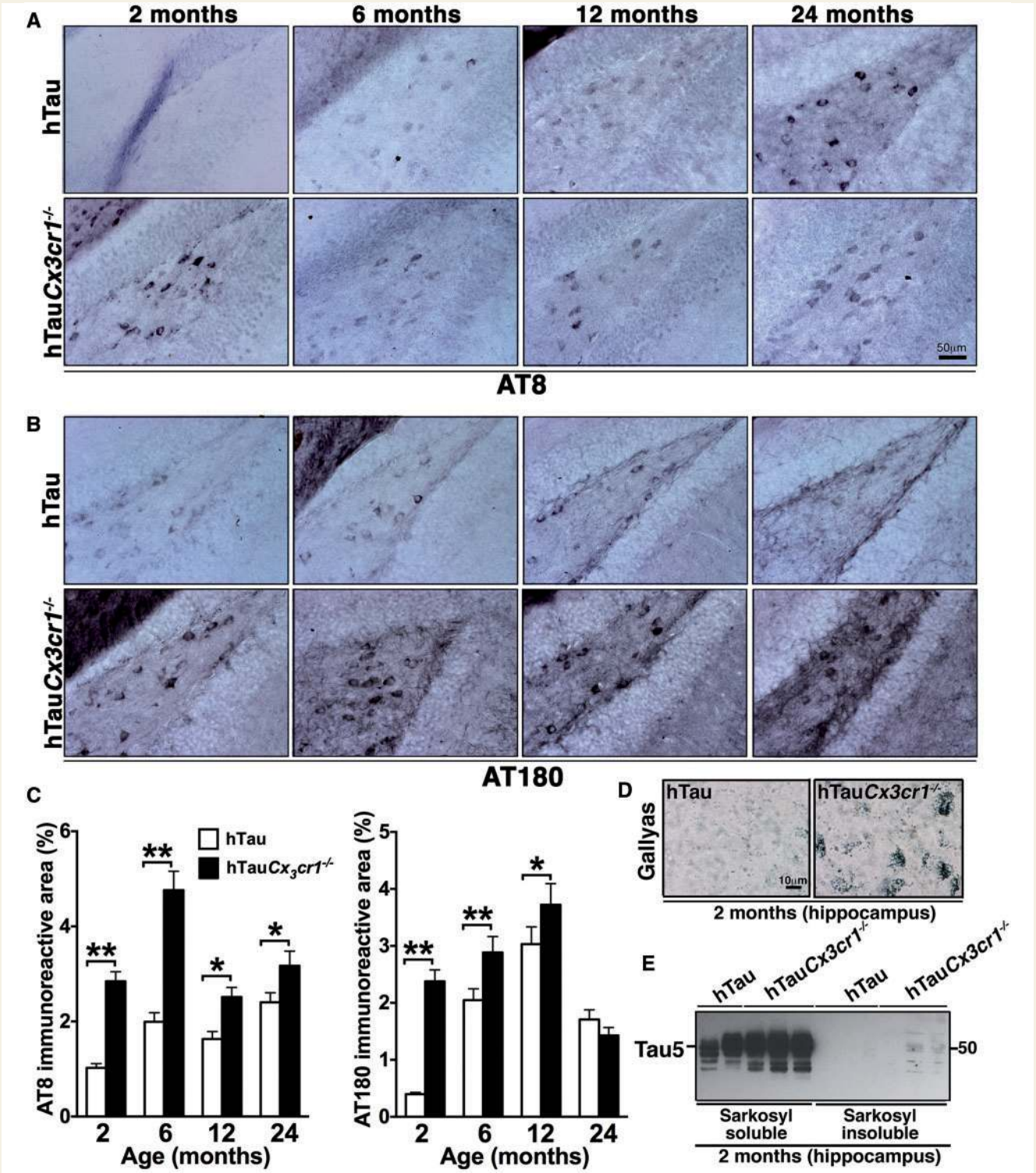

Figure 2 Early onset and progression of tau pathology in the hippocampus of hTau*Cx3cr1*$^{-/-}$ mice. (**A** and **B**) Immunohistochemical analysis (using Sigma-Fast DAB with $CoCl_2$-metal enhancement therefore appears dark purple) shows presence of numerous AT8$^+$ and AT180$^+$ neurons in the dentate gyrus of 2- and 6-month-old hTau*Cx3cr1*$^{-/-}$ mice compared to age-matched hTau mice. By 6 months of age, hTau mice also show both AT8$^+$ and AT180$^+$ neurons. Scale bar = 50um (**A** and **B**). (**C**) Quantitative morphometric analysis shows a significant increase in AT8$^+$ and AT180$^+$ neurons in hTau*Cx3cr1*$^{-/-}$ mice from 2- to 12-months of age with an overall drop in AT8$^+$ neurons at 12 months and AT180$^+$ neurons at 24 months of age mean ± SEM immunoreactive area ratio of respective epitopes (**C**). (**D**) Gallyas silver positive pre-tangle aggregates (appeared intraneuronal) are evident in the CA1 neurons of hippocampus of 2-month-old hTau*Cx3cr1*$^{-/-}$ mice compared to hTau mice. Scale bar = 10 μm. (**E**) Sarkosyl insoluble tau is evident in the hippocampi of 2-month-old hTau*Cx3cr1*$^{-/-}$ mice compared to age-matched hTau mice.

aggregation of tau, we performed Sarkosyl insoluble assay in the hippocampus of 2-month-old hTau and hTau*Cx3cr1*$^{-/-}$ mice. Notably, while the total tau (Tau5^{+}) was present in the Sarkosyl soluble fractions of both hTau and hTau*Cx3cr1*$^{-/-}$ mice (Fig. 2E), Sarkosyl-insoluble tau was present only in hTau*Cx3cr1*$^{-/-}$ mice (Fig. 2E). Taken together, these results suggest that deficiency of microglial CX3CR1 in hTau mice leads to enhanced tau phosphorylation and pre-tangle aggregation as early as 2 months of age.

Reduced SNAP25 levels, abnormal CA1 neuronal architecture and spatial memory impairment and neuronal loss in the hTau*Cx3cr1*$^{-/-}$ mice

To determine whether build-up of pathological tau in the hTau*Cx3cr1*$^{-/-}$ mice results in altered synaptic and neuronal structure, we assessed the expression of various synaptic proteins (synaptophysin, syntaxin, synapsin and SNAP25) and the neuronal marker NeuN within the hippocampus. Although we did not detect significant alterations in the levels of synaptophysin, syntaxin and synapsin, the level of SNAP25 was significantly reduced from 6 months to 12 months only in the hTau*Cx3cr1*$^{-/-}$ mice compared to hTau mice (Fig. 3A and B). Notably, the thickness of NeuN^{+} cells in a stereologically identical region of the CA1 subfield was markedly thinner in hTau*Cx3cr1*$^{-/-}$ mice at 2 months of age compared to age-matched hTau and non-transgenic mice (Fig. 3C). Finally, as the hTau*Cx3cr1*$^{-/-}$ mice aged, the wet weight of the hippocampus was significantly reduced compared to hTau mice (Fig. 3D). Together, these data suggest that the hippocampus is affected in hTau*Cx3cr1*$^{-/-}$ mice as early as 2 months of age and this worsens with age.

We have previously demonstrated that *Cx3cr1* deficiency leads to working memory impairment in the 6-month-old hTau mice (Bhaskar *et al.*, 2010). To further assess hippocampal-dependent learning and memory, hTau and hTau*Cx3cr1*$^{-/-}$ mice were compared with non-transgenic mice for spatial memory in the Morris Water Maze at 6 and 12 months of age. First, the mice were trained for 3 days to escape to a visible platform in a cued paradigm (the mice use visual cues to seek the platform) and the escape latency (time to reach the platform) was calculated. Both hTau and hTau*Cx3cr1*$^{-/-}$ mice displayed longer escape latencies on the second day of training (Fig. 3E, 'Visible Platform'). Notably, statistical analysis with group-wise comparisons revealed that on Day 2, both hTau and hTau*Cx3cr1*$^{-/-}$ mice took a significantly longer time to learn to reach the platform as compared to non-transgenic mice (Fig. 3E). By the third day, there was no difference observed in the escape latency among different groups. For the next four consecutive days, we tested these mice in the hidden-platform paradigm of Morris Water Maze. While non-transgenic animals showed a decrease in escape latency (time required to reach the hidden platform), hTau and hTau*Cx3cr1*$^{-/-}$ mice took much longer to reach the hidden platform (Fig. 3E). Two-way ANOVA followed by Tukey's multiple comparisons revealed statistically significant delays in finding the hidden platform for hTau (on Day 4) and hTau*Cx3cr1*$^{-/-}$ mice (on Day 7) compared to non-transgenic control groups (Fig. 3E). Interestingly, two-way ANOVA with repeated measures comparing the mean latency between different testing days within each genotype suggested that non-transgenic and hTau mice showed differences in latency with highest statistical significance ($***P < 0.0001$) compared to hTau*Cx3cr1*$^{-/-}$ mice ($*P < 0.05$) between Days 4 and 7, suggesting that the latency in hTau*Cx3cr1*$^{-/-}$ mice plateaus from Day 5 to day 7 (Fig. 3E). Furthermore, no significant differences were observed with respect to swim speed, total distance travelled, proximity to platform and probe test among different groups of mice tested. In summary, these results suggest that while hTau and hTau*Cx3cr1*$^{-/-}$ mice display variations in their learning abilities compared to non-transgenic mice; their latencies appear to plateau (primarily for hTau*Cx3cr1*$^{-/-}$ mice on Day 7), suggesting a possible impairment in retention or consolidation in hTau*Cx3cr1*$^{-/-}$ mice at 6 months of age.

Next, we tested 12-month-old cohorts of mice on both cued and hidden versions of the Morris Water Maze. Notably, no significant difference was observed in the escape latency when two-way ANOVA with multiple comparisons were performed. However, both hTau and hTau*Cx3cr1*$^{-/-}$ mice displayed significant impairment (Fig. 3F) in proximity to platform [referred to as 'Proximity Measure' or 'Gallagher's measure' (Gallagher *et al.*, 1993)], which is one of the most sensitive tests to assess cognitive function (Maei *et al.*, 2009). Finally, in the probe test, only hTau*Cx3cr1*$^{-/-}$ mice spent less time in the target quadrant (Fig. 3G) and displayed a statistically significant impairment compared to age-matched non-transgenic controls (Fig. 3H). Taken together, these results suggest that deficiency of *Cx3cr1* in hTau mice leads to notable alterations in the spatial memory function as early as 6 months of age, which is more pronounced at 12 months of age.

To assess if the behavioural impairment observed in hTau*Cx3cr1*$^{-/-}$ mice was related to neuronal cell loss, we performed immunohistochemistry and quantitative morphometry for the neuron-specific antigen NeuN in 12-month-old non-transgenic, hTau and hTau*Cx3cr1*$^{-/-}$ groups of mice (Supplementary Fig. 3). Earlier studies have suggested that hTau mice show significant reductions in the number of neurons in the piriform cortex at 17 months of age (Andorfer *et al.*, 2005). Based on this, we performed immunohistochemical and quantitative analysis in layer II of the piriform cortex. The NeuN^{+} neurons were dense with several layers of cells in 12-month-old non-

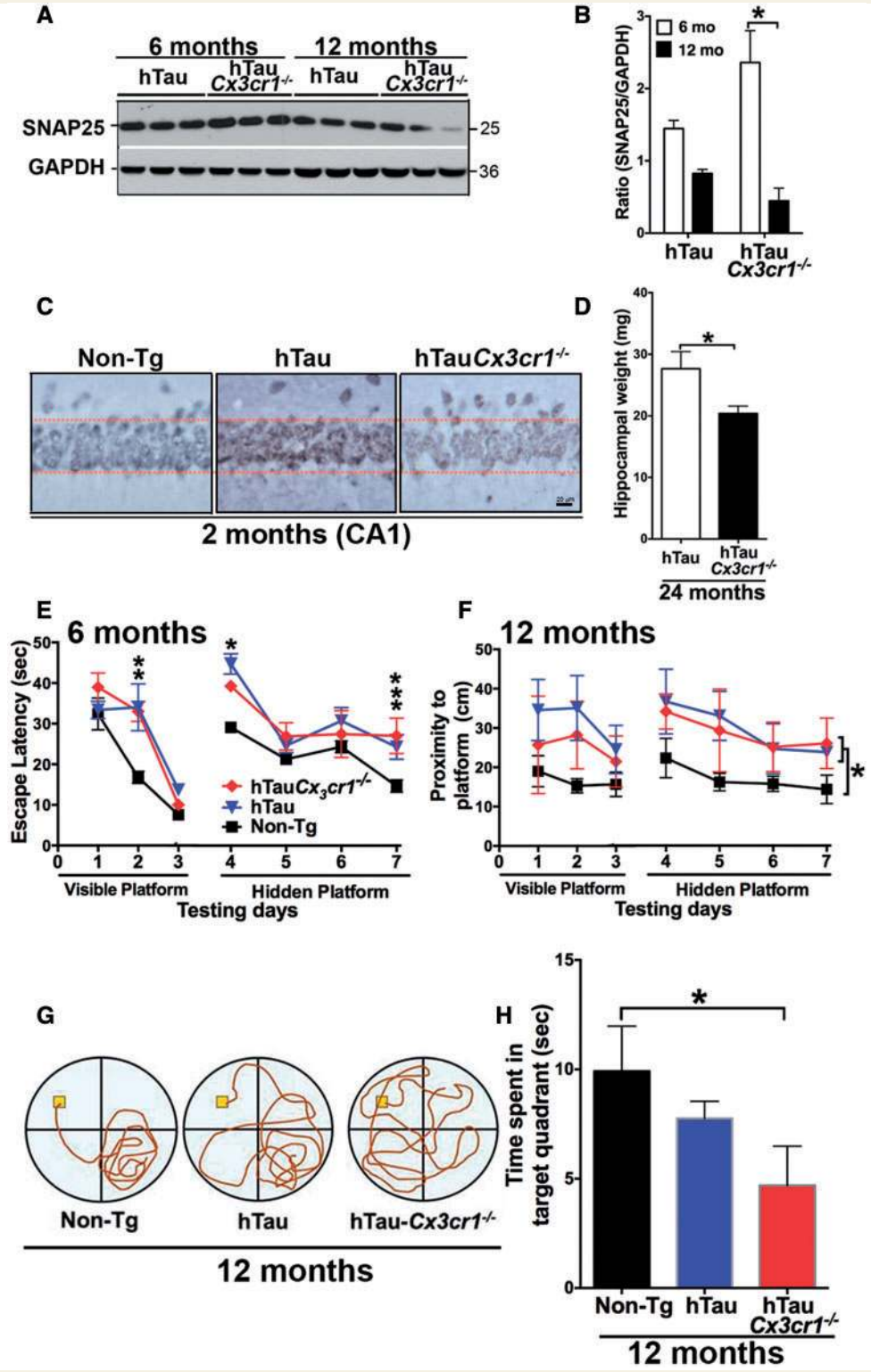

Figure 3 Reduced SNAP25 levels, neuronal abnormality and impaired spatial memory in the hTau*Cx3cr1*$^{-/-}$ mice. (**A** and **B**) Western blot analysis of hippocampal lysates reveal reduced SNAP25 levels in the 6-month-old hTau*Cx3cr1*$^{-/-}$ mice. Quantification of western blots for SNAP25 and GAPDH revealed a statistically significant (*$P < 0.05$ for 12-month-old hTau*Cx3cr1*$^{-/-}$ mice versus 6-month-old hTau*Cx3cr1*$^{-/-}$ mice; $n = 3$; mean ± SEM of SNAP25/GAPDH ratio; unpaired *t*-test) decrease in the SNAP25 from 6 months to 12 months of age in hTau*Cx3cr1*$^{-/-}$ mice. (**C** and **D**) Thickness of the NeuN^{+}CA1 layer appears reduced in the identical region of the CA1 subfield in the 2-month-old hTau*Cx3cr1*$^{-/-}$ mice. Scale bar = 20 μm. Wet weights of hippocampi were significantly (*$P < 0.05$; $n = 5$; mean ± SEM; unpaired *t*-test) lower in the 24-month-old hTau*Cx3cr1*$^{-/-}$ mice compared to age-matched hTau mice. (**E–H**) Visible and hidden platform versions of the Morris Water Maze. (**E**) At 6-months of age: mean latency to escape to a visible or hidden platform across training days was assessed from Day 1 through to Day 7. Note statistically significant differences (**$P < 0.01$ for hTau*Cx3cr1*$^{-/-}$ and *$P < 0.05$ for hTau mice versus non-transgenic mice on Day

(continued)

transgenic brains (Supplementary Fig. 3A), wereas the NeuN$^+$ neurons in hTau mice appeared dysmorphic, but the density was only slightly lower compared to non-transgenic piriform cortex (Supplementary Fig. 3B). There was a reduced density of NeuN$^+$ cells in hTau*Cx3cr1*$^{-/-}$ mice compared to non-transgenic and hTau mice (Supplementary Fig. 3C). Upon quantification of the NeuN$^+$ area fraction, there was a statistically significant decrease in the 12-month-old hTau*Cx3cr1*$^{-/-}$ mice compared to non-transgenic controls (Supplementary Fig. 3D). These results, along with thinner CA1 layer in the 2-month-old hTau*Cx3cr1*$^{-/-}$ mice (Fig. 3C), suggest that deficiency of microglial CX3CR1 in hTau*Cx3cr1*$^{-/-}$ mice induces neurodegeneration, which occurs several months prior to significant neuronal loss demonstrated in the hTau mice (12 months versus 17 months of age) (Andorfer *et al.*, 2005).

Microglial activation in pre-pathological hTau*Cx3cr1*$^{-/-}$ mice

To determine whether microglial activation precedes or follows tau hyperphosphorylation and aggregation, we performed immunohistochemical and biochemical analysis in 2-month-old hTau and hTau*Cx3cr1*$^{-/-}$ mice. Iba1$^+$ microglia displayed activated morphology in the CA3 regions of hTau*Cx3cr1*$^{-/-}$ mice at 2 months of age compared to hTau mice (Fig. 4A). Based on our previous observation that IL1R1 knockout (*Il1r1*$^{-/-}$) mice were resistant against lipopolysaccharide-induced tau hyperphosphorylation and that blocking IL1R1 prevented microglia-induced tau phosphorylation *in vitro* (Bhaskar *et al.*, 2010), we next studied the mRNA and protein levels of active IL1B. Notably, quantitative real-time PCR analysis revealed a significant increase in *Il1b* mRNA levels in hTau*Cx3cr1*$^{-/-}$ mice compared to non-transgenic control mice at 2 months of age (Fig. 3B). Three distinct steps tightly control the production of IL1B (Burns *et al.*, 2003). The first step involves the production of the pro-IL1B protein (p35); this is followed by cleavage of pro-IL1b by caspase 1 to produce the active IL1b protein (p17); which then is released into the extracellular space (Burns *et al.*, 2003). The processing of pro-IL1b involves the activation of a caspase 1-activating complex, known as the 'inflammasome' (Lamkanfi and Dixit, 2009). Similar to IL1b, caspase 1 itself undergoes cleavage to produce p20 (20 kDa) and p10 (10 kDa) activation forms that are recruited to the inflammasome complex for the processing of pro-IL1b. Elevated levels of pro-IL1b were observed in both hTau and hTau*Cx3cr1*$^{-/-}$ mice at 2 months of age (Supplementary Fig. 4A). Upon quantification, an increase in the mean ratio of pro-IL1b/GAPDH was observed in both hTau and hTau*Cx3cr1*$^{-/-}$ mice compared to non-transgenic mice (Supplementary Fig. 4A and B), but the hTau*Cx3cr1*$^{-/-}$ mice differed with higher statistical strength than hTau mice (Supplementary Fig. 4B). While the levels of cleaved (active form) IL1b were indistinguishable from 2-month-old hTau*Cx3cr1*$^{-/-}$ mice compared to hTau mice on a western blot analysis, the levels of p10 cleaved fragment of active caspase 1 were significantly higher in 2-month-old hTau*Cx3cr1*$^{-/-}$ mice compared to age-matched hTau mice (Supplementary Fig. 4A and C). To confirm that activation of caspase 1 is leading to maturation of IL1b, we performed an active IL1b assay using HEK-Blue^{TM} reporter cells. The HEK-Blue^{TM} reporter cell assay (Invivogen) USES a cell line that expresses IL1R1 (interleukin 1 receptor, type 1), a cognate receptor exclusively for mature IL1B (Fig. 4C). The activation of IL1R1 leads to engagement of MYD88 adapter protein and activation of NF-κB complex to lead to the transcription of SEAP reporter (Fig. 4C) in the media. Levels of SEAP in the media reflect the absolute level of IL-1b in the test samples. This assay is considerably more sensitive than western blot analysis. Soluble lysate from 2-month-old hTau*Cx3cr1*$^{-/-}$ mice displayed a significant increase in the levels of active IL1B HEK-Blue^{TM} reporter cell assay compared to age-matched non-transgenic mice (Fig. 4D), suggesting the activation of the IL1B pathway in hTau*Cx3cr1*$^{-/-}$ mice as early as 2 months of age.

Next we assessed the expression of CD68—a surface marker of phagocytic cells. There was no difference in the CD68 immunoreactivity in 2-month-old hTau*Cx3cr1*$^{-/-}$ mice compared to 2-month-old non-transgenic via immunohistochemical analysis (Supplementary Fig. 4D and E). The 24-month-old hTau*Cx3cr1*$^{-/-}$ mice showed a marked increase in CD68 in the hippocampus compared to age-matched non-transgenic mice (Supplementary Fig. 4D and E). Upon quantification, the CD68 immunoreactive area was significantly higher in 24-month-old hTau*Cx3cr1*$^{-/-}$ mice compared to age-matched non-transgenic mice (Supplementary Fig. 4E). A statistically significant increase in the *CD68* mRNA levels was observed in 2-month-old hTau*Cx3cr1*$^{-/-}$ mice compared to age-matched non-transgenic mice in the

Figure 3 Continued

2; *$P < 0.05$ for hTau versus non-transgenic on Day 4; **$P < 0.01$ for hTau*Cx3cr1*$^{-/-}$ versus non-transgenic on Day 7; two-way ANOVA with Tukey's multiple comparison test; $n = 7$; mean ± SEM) in the mean escape latency on Days 2, 4 and 7. (**F**) At 12 months of age: platform proximity during visible and hidden training sessions are significantly (*$P < 0.05$ for hTau and hTau*Cx3cr1*$^{-/-}$ mice versus non-transgenic comparing mean ± SEM of three trials for each day; two-way ANOVA with Tukey's—for the platform proximity; $n = 6$) altered in hTau and hTau*Cx3cr1*$^{-/-}$ mice compared to non-transgenic mice. (**G** and **H**) At 12 months of age: representative traces showing swim pattern of different groups of mice during probe test (when the hidden platform was removed and the time spent in target quadrant was assessed). *Bottom right* is the target quadrant. A probe test on Day 8 revealed only 12-month-old hTau*Cx3cr1*$^{-/-}$ mice spending significantly less time in the target quadrant (*$P < 0.05$ for hTau*Cx3cr1*$^{-/-}$ mice versus non-transgenic; one-way ANOVA with Tukey's multiple comparison test; $n = 6$; mean ± SEM).

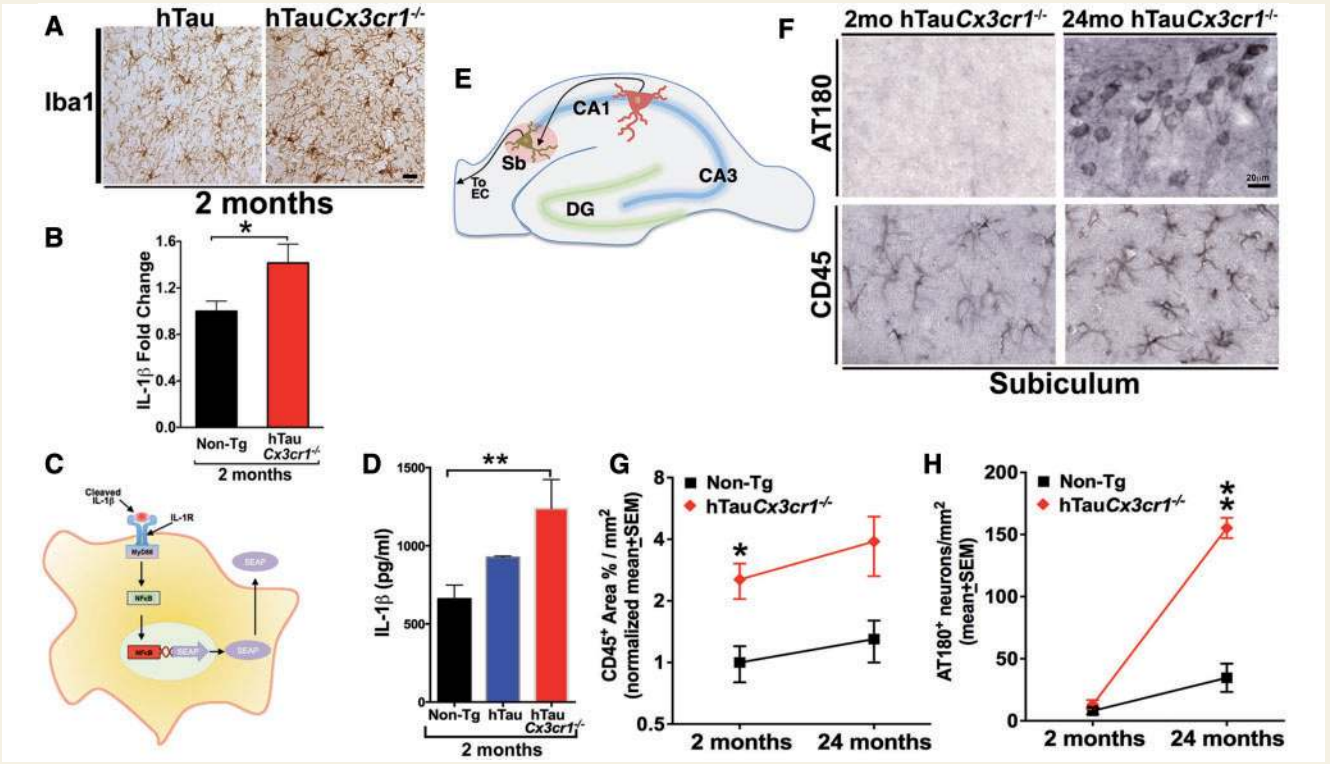

Figure 4 Microglial activation and IL1B maturation precedes spreading of tau pathology in hTau*Cx3cr1*$^{-/-}$ mice.
(**A**) Iba1^{+} microglia in the CA3 region of hippocampus of 2-month-old hTau and hTau*Cx3cr1*$^{-/-}$ mice. Scale bar = 10 μm. (**B**) Quantitative real-time PCR analysis of *Il1b* transcript levels reveal a significant (*$P < 0.05$; $n = 5$; mean ± SEM; unpaired *t*-test) increase in IL1B expression in the hemi-brains of 2-month-old hTau*Cx3cr1*$^{-/-}$ mice compared to age-matched non-transgenic controls. (**C** and **D**) Mature/active IL1B is present at elevated levels in hTau*Cx3cr1*$^{-/-}$ mice as early as 2 months of age. Overnight stimulation of HEK-Blue^{TM} IL1B reporter cells (InvivoGen) with detergent (T-PER, Pierce) soluble hippocampal lysates from 2-month-old non-transgenic, hTau and hTau*Cx3cr1*$^{-/-}$ mice show significantly (**$P < 0.01$ one-way ANOVA with Tukey's multiple comparison test; $n = 3$ mice per group; mean ± SEM) increased production of SEAP (NF-κB/AP-1-inducible SEAP reporter gene that is activated when mature IL1B in the lysate binds to IL1R1 on the surface of HEK-Blue^{TM} IL1B cells). SEAP levels in the media were measured by QUANTI-Blue^{TM} assay at 620 nm. (**B–D**) Levels of full-length and cleaved IL1B (17 kDa) are significantly higher in hTau*Cx3cr1*$^{-/-}$ mice (quantification for pro-IL1B/GAPDH in (**C**) **C**: *$P < 0.05$ for hTau mice and **$P < 0.01$ for hTau*Cx3cr1*$^{-/-}$ mice versus non-transgenic; for cleaved IL1B/GAPDH ratio in (**D**) **D**: *$P < 0.01$ for hTau*Cx3cr1*$^{-/-}$ versus non-transgenic mice. One-way ANOVA with Tukey's multiple comparison; $n = 3$; mean ± SEM]. (**E**) Schematic showing hippocampal circuitry where subiculum (Sb) receives input from the CA1 and sends out projections to entorhinal cortex (EC). Shaded region (light red) shows the area where morphometric analysis was performed in subiculum. (**F**) CD45 reactive microglia are present in the subiculum of hTau*Cx3cr1*$^{-/-}$ mice as early as 2 months of age, however, the AT180^{+} tau is almost not detectable in the lateral subiculum at 2 months of age. More robust staining for CD45 and AT180 is apparent in the subiculum of 24-month-old hTau*Cx3cr1*$^{-/-}$ mice. Scale bars = 20 μm (all frames). (**G** and **H**) Quantification of CD45 immunoreactive area (**G**) and number of AT180^{+} neurons (**H**). Note, CD45 immunoreactive area, but not the number of AT180^{+} neurons, is significantly higher in hTau*Cx3cr1*$^{-/-}$ mice (*$P < 0.05$ for 2-month-old hTau*Cx3cr1*$^{-/-}$ versus non-transgenic; unpaired *t*-test; $n = 4$; mean ± SEM).

real-time quantitative PCR analysis (Supplementary Fig. 4F). Together, these results suggest that Iba1^{+} microglial activation, caspase-1 (inflammasome) activation, maturation of IL1B and CD68 expression, correlate with early stages of tau pathology in the hTau*Cx3cr1*$^{-/-}$ mice.

Microglial activation correlates with the spread of tau pathology in the anatomically connected regions of the hippocampus

Recent evidence suggests that pathologically misfolded and hyperphosphorylated tau can spread like 'prions' via anatomically connected regions of the brain (Frost *et al.*, 2009; Liu *et al.*, 2012). To determine if microglial activation correlates with the spread of tau pathology we examined the subicular region of the hippocampus in 2- and 24-month-old hTau*Cx3cr1*$^{-/-}$ mice. The subiculum (Sb) acts as a relay centre between the projections from the CA1 and the entorhinal cortex (Fig. 4E). The axonal projections from CA1 neurons to the subiculum and onward to the entorhinal cortex form the principal output for the hippocampus and follow a strict anatomical layout. The distal end of the CA1 neurons projects to the proximal end (dendrites) of subiculum neurons (Fig. 4E) thus it provides an opportunity to study the anterograde-based spread of tau pathology. First, only the CA1 neurons of the

hippocampus were positive for AT180 in the 2-month-old hTau*Cx3cr1*$^{-/-}$ mice, while the subiculum showed very few neurons positive for AT180 (Fig. 4F and Supplementary Fig. 2A). Adjacent sections stained with CD45, a cell surface marker for activated microglia (Ho *et al.*, 2005), showed a substantial number of CD45^{+} microglia within the identical subregions of the subiculum (Fig. 4F). By 24 months of age, a majority of subiculum neurons displayed AT180 immunoreactivity (Fig. 4F) in the hTau*Cx3cr1*$^{-/-}$ mice and this was spatiotemporally correlated with substantial CD45 immunoreactivity in the identical region (Fig. 4F, CD45 and AT180). Notably, a majority of CD45^{+} microglia displayed activated morphology (Fig. 4F). Finally, quantitative analysis revealed that the per cent area immunoreactive for CD45^{+} in the subiculum of hTau*Cx3cr1*$^{-/-}$ mice was significantly higher as early as 2 months of age than those from age-matched non-transgenic mice (Fig. 4G). Interestingly, while a very small portion of AT180 positive neurons were present in the subiculum of 2-month-old hTau*Cx3cr1*$^{-/-}$ mice, their number was not significantly higher than those in the non-transgenic group (Fig. 4H). We observed a similar trend in AT8^{+} neurons in the subiculum of 2- versus 24-month-old hTau*Cx3cr1*$^{-/-}$ mice. Notably, the subiculum of hTau*Cx3cr1*$^{-/-}$ mice was devoid of any AT8^{+} neurons at 2 months of age (Supplementary Fig. 5)—a time point at which numerous CD45^{+} cells are already present in the subiculum (Fig. 4F and G). Together, these results suggest that microglial activation may precede the spreading of pathological AT180^{+} and AT8^{+} tau in anatomically connected regions of the hTau*Cx3cr1*$^{-/-}$ mouse hippocampus. Therefore, microglia may participate in 'seeding' and/or 'spreading' of pathological (specifically AT8^{+} and AT180^{+}) tau species.

Activated microglia induce tau pathology

If CD45^{+} microglial activation precedes the induction of AT8/AT180 site tau phosphorylation, then isolation and administration of such reactive microglia (independent of other CNS cell types) may also be able to induce tau hyperphosphorylation and aggregation inside the brains of naïve, non-transgenic mice. To test this, a series of adoptive transfer experiments were performed. First, *Cx3cr1*$^{-/-}$ microglia (GFP positive because of targeted insertion of GFP into *Cx3cr1* locus—Fig. 5A) derived from primary microglial cultures were directly injected in to the brains of 2-month-old non-transgenic mice. Seventy-two hours following microglial administration, recipient brains were examined for the presence of GFP^{+} donor microglia. Numerous AT8^{+} dystrophic neurites/processes and cell bodies were detected around the needle track (Fig. 5B). No significant alterations in the AT8 immunoreactivity were observed in the contralateral side (data not shown).

In the next set of experiments, microglia from 6-month-old non-transgenic, hTau and hTau*Cx3cr1*$^{-/-}$ mice were purified using an established protocol (Bergmann *et al.*, 1999) with minor modifications that included CD11b antibody mediated enrichment of reactive microglia/macrophages (Bhaskar *et al.*, 2014) (Fig. 5C). Purified microglia were microinjected (50 000 cells/injection) into the cortical layer VI of 6-month-old non-transgenic (isogenic) recipient mouse brain (Fig. 5C). Seventy-two hours after adoptive transfer, recipient brains were analysed for the presence of donor microglia within 1–2 mm radius of the needle track. Recipient mice that received hTau*Cx3cr1*$^{-/-}$ microglia displayed numerous GFP^{+} donor microglia within several millimetres surrounding the tip of the needle track (small white square in Fig. 5D) and they appear activated (Fig. 5D, square inset). Interestingly, the majority of injected microglia have localized to layer VI of the cortex, dorsal caudate-putamen and several of them tangentially migrated via the corpus callosum (Fig. 5D, rectangle inset). Immunohistochemical analysis in the caudate-putamen area of the non-transgenic mice that received vehicle revealed very few AT8^{+} dystrophic neurites (due to needle-injury induced dystrophy) AT8 and no obvious cellular labelling of AT8 (Fig. 5E). On the other hand, non-transgenic recipients that received microglia derived from non-transgenic donors displayed some AT8^{+} dystrophic neurites and some AT8 immunoreactivity appeared intracellular (Fig. 5F). Notably, an increase in AT8^{+} dystrophic neurites and cellular staining was observed in non-transgenic recipients that received microglia from hTau donors (Fig. 5G). This trend was more robust in the recipients that received microglia from hTau*Cx3cr1*$^{-/-}$ donor mice (Fig. 5H). Notably, some of the pyramidal neurons around the needle track in the cortical region also showed intracellular AT8 labelling (Fig. 5H, inset). To determine if adoptive transfer of reactive microglia also induced AT180-site phosphorylation in the mouse tau within the brains of non-transgenic mice, adjacent brain sections of non-transgenic recipients that received hTau*Cx3cr1*$^{-/-}$ microglia were stained for AT180. Robust AT180 reactivity was present inside striatal and layer VI of cortical neurons (Supplementary Fig. 6A and B) of recipient mice. Furthermore, similar to AT8^{+} dystrophic neurites, numerous AT180^{+} dystrophic neurites were observed at the site of injection within the striatum (Supplementary Fig. 6C).

Next, to test whether AT8 immunoreactivity spatially overlaps with the presence of reactive microglia from hTau*Cx3cr1*$^{-/-}$ donors within the brains of recipients, we performed confocal double immunofluorescence analysis for GFP and AT8 (Fig. 5I–K). Interestingly, AT8^{+} dystrophic neurites and cellular structures spatially co-existed near GFP^{+} donor microglia (Fig. 5I–K). Notably, many of the AT8^{+} cells were neurons in the layer VI of the cortex (Supplementary Fig. 7A and B). Confocal 3D reconstruction of 15-μm thick brain slice of the field shown in Supplementary Fig. 7B suggested a clear induction of AT8

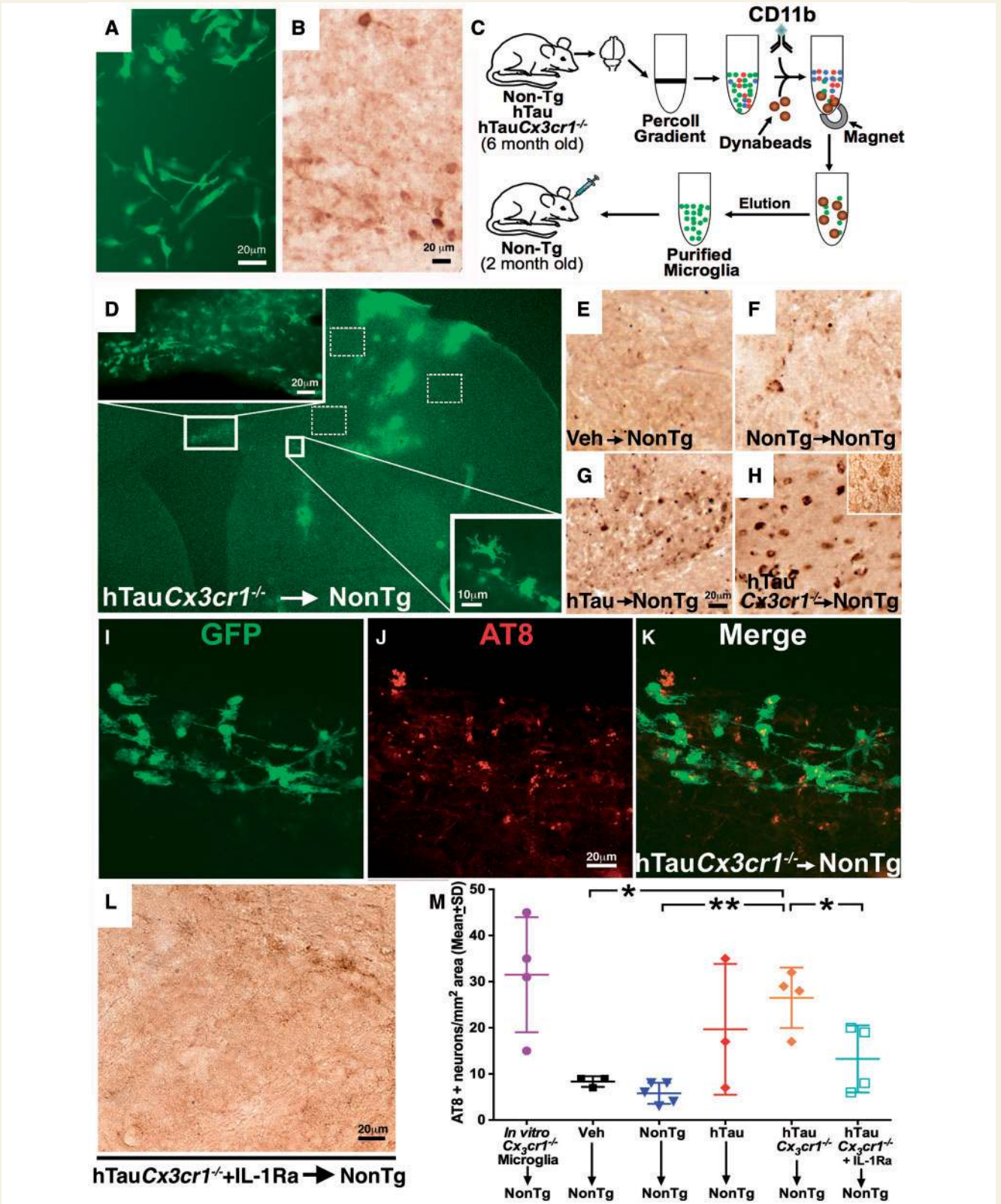

Figure 5 Adoptive transfer of purified microglia from hTau*Cx3cr1*$^{-/-}$ mice induces tau hyperphosphorylation *in vivo*. (**A**) GFP^{+} *Cx3cr1*$^{-/-}$ microglia 14 days *in vitro* in primary culture. Scale bar = 20 μm. (**B**) A representative image showing AT8 immunoreactivity in the striatum of a naïve non-transgenic recipient mouse that received GFP^{+} *Cx3cr1*$^{-/-}$ microglia from primary cultures. Scale bar = 20 μm. (**C**) Schematic showing the magnetic-based isolation of CD11b^{+} microglia and intracerebral injections of purified microglia into the recipient mouse brain. (**D**) A representative low magnification image showing a needle track from the brain surface through layer VI of the cortex and parts of the carpus callosum. GFP^{+} microglia from hTau*Cx3cr1*$^{-/-}$ mice are viable, appear activated and have migrated several hundreds of microns away from

(continued)

site hyperphosphorylation of endogenous mouse tau within several neurons that surround GFP$^+$ microglia from hTau*Cx3cr1*$^{-/-}$ donor mice (Supplementary Video 1). Based on our previous work (Bhaskar *et al.*, 2010) and present observation (Fig. 4B–D) that IL1B secreted from activated microglia may drive inflammation-induced tau hyperphosphorylation, we tested the effect of intereleukin-1 receptor antagonist (IL-1Ra or Kineret®), which is known to compete with IL1B and block IL-1R activation (Clark *et al.*, 2008). Inclusion of IL-1Ra with the inoculum of hTau*Cx3cr1*$^{-/-}$ microglia resulted in complete elimination of AT8 immunoreactive structures within the recipient mouse brain (Fig. 5L). Next, to determine whether hyperphosphorylation of endogenous tau within the recipient mouse brain leads to the formation of silver positive pre- or mature-tangles, we performed Gallyas silver staining. Non-transgenic mice receiving either vehicle or microglia from non-transgenic donors did not display any silver positive structures/cells (Supplementary Fig. 7C and D). While 72 h post-inoculation is too early to expect any silver positive neurons/dystrophic neurites within the recipient mouse brain, we did observe diffuse peri-nuclear staining in a small population of striatal neurons of the mice receiving microglia from hTau donors (Supplementary Fig. 7E). The intensity of silver staining was more obvious in the striatal and cortical neurons of the recipient mice that received microglia from hTau*Cx3cr1*$^{-/-}$ donors (Supplementary Fig. 7F and inset). However, these silver positive neurons were very few in number (in the striatum right around the area of needle tip) and appeared to contain early stages of tau aggregates compared to typical tangle-bearing neurons found in human Alzheimer's disease brain (Supplementary Fig. 7G and inset). Notably, the mice inoculated with hTau*Cx3cr1*$^{-/-}$ donor microglia along with IL-1Ra showed no silver positive cells/dystrophic neurites (Supplementary Fig. 7H). Next, we performed quantitative analysis of multiple coronal free-floating brain sections from the recipient mice to examine AT8$^+$ neurons/intracellular immunoreactivities. We scored four random fields 1–2 mm area on either side of the needle track in four sections per mice (n = 3–5 recipient mice per group). Recipients that received *Cx3cr1*$^{-/-}$ microglia derived from primary cultures showed 20–40 AT8$^+$ neurons per mm^2, while those that received vehicle alone or microglia from non-transgenic donors displayed $<$10 AT8$^+$ neurons within the same defined area (Fig. 5M). Remarkably, microglia derived from hTau mice resulted in a notable increase in the number of AT8$^+$ neurons. The most significant increase was observed in the recipients of hTau*Cx3cr1*$^{-/-}$ microglia that show a statistically significant increase in the number of AT8$^+$ neurons compared to those receiving vehicle or non-transgenic microglia (Fig. 5M). Inclusion of IL1-Ra into the hTau*Cx3cr1*$^{-/-}$ microglial inoculum reduced the number of AT8$^+$ neurons by nearly 50% (Fig. 5M). Finally, to determine if the effect of IL-1Ra on reduced AT8 and AT180 site tau phosphorylation is mediated via downregulation of p-p38 MAPK, we performed immunohistochemical and triple immunofluorescence analysis for p-p38 MAPK alone or with DAPI and GFP$^+$ donor microglial cells. Notably, numerous p-p38 MAPK positive cells (majority of them non-neuronal) were apparent in the area around the needle track (Fig. 6A) and surrounding GFP$^+$ donor microglia (Fig. 6C) in the non-transgenic mice receiving hTau*Cx3cr1*$^{-/-}$ microglia. In contrast, mice receiving hTau*Cx3cr1*$^{-/-}$ microglia + IL-1Ra displayed markedly reduced number of p-p38 MAPK positive cells in the identical region around the needle track (Fig. 6B). Notably, such reduction in p-p38 MAPK immunoreactivity was also observed around GFP$^+$ donor microglia (Fig. 6D). Quantification of the percent area positive for p-p38 MAPK (from the bright field immunohistochemical images) reveal a statistically significant reduction in the mice receiving hTau*Cx3cr1*$^{-/-}$ microglia + IL-1Ra compared to hTau*Cx3cr1*$^{-/-}$ microglia alone (Fig. 6E). Taken together, these results suggest that reactive microglia derived from either an *in vitro* source or from hTau*Cx3cr1*$^{-/-}$ mice are sufficient and can directly induce AT8 and AT180 site hyperphosphorylation of endogenous mouse tau that can be blocked by an IL-1Ra via reduced activation of p38 MAPK.

Figure 5 Continued

the injection site (green in the insets). Boxes with dashed line show representative areas where quantifications were done (for panel **M**). Scale bars = 20 μm (*top left inset*) and 10 μm (*bottom right inset*). (**E–H**) Microglia derived from 6-month-old hTau*Cx3cr1*$^{-/-}$ mice induce robust AT8$^+$ staining in neurons/dystrophic neurites within the striatum of 2-month-old non-transgenic recipient mouse brain (**H**) compared to those derived from non-transgenic (**F**) or hTau (**G**) donor mice and RPMI media (vehicle) injected mice (**E**). hTau*Cx3cr1*$^{-/-}$ microglial recipients also showed several AT8$^+$ pyramidal neurons around the needle track in the cortex (inset in **H**). Scale bar = 20 μm. (**I–K**) Representative confocal images showing hTau*Cx3cr1*$^{-/-}$ donor microglia within the recipient mouse brain (**I**) and the majority of them appear activated. In the same field, certain dystrophic neurites and cells show AT8 positivity (**J** and **K**). Scale bar = 20 μm. See also Supplementary Figs 5 and 6. (**L**) Inclusion of IL-1Ra with the hTau*Cx3cr1*$^{-/-}$ microglial inoculum shows no AT8 immunoreactive dystrophic structures/neurons within the recipient mice. Scale bar = 20 μm. (**M**) Quantification of AT8$^+$ neurons/mm^2 revealed a statistically significant (n = 3–5 recipients per treatment; five sections per mouse; six random fields per section were scored; mean ± SD; *$P < 0.05$; **$P < 0.001$; one-way ANOVA with a Tukey's multiple comparison test; each marker represent individual recipient mouse) increase in AT8$^+$ neurons in the ipsilateral cortex of recipient mouse brain that received (i) primary *Cx3cr1*$^{-/-}$ microglia (purple data set); and (ii) microglia from 6-month-old hTau*Cx3cr1*$^{-/-}$ donor mice (brown data set). Vehicle injected or those receiving microglia from 6-month-old non-transgenic or hTau donors did not show AT8$^+$ neurons (black, blue and red data sets). Inclusion of IL-1Ra in the inoculum significantly reduced the number of AT8$^+$ neurons (turquoise data set).

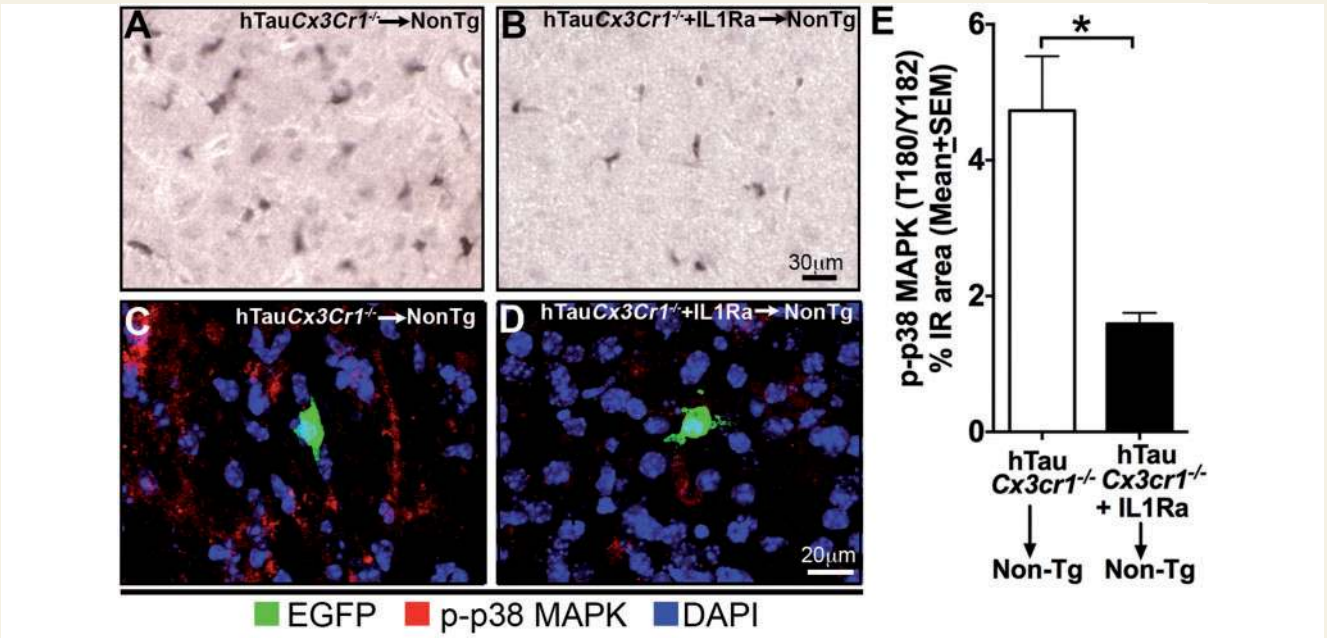

Figure 6 Inclusion of IL-1Ra in the microglial inoculum reduces overall reactivity for phosphorylated p38 MAPK within the recipient mouse brain. (**A**, **B** and **E**) Immunostained brain sections displaying overall reduced phosphorylated (p)-p38 MAPK (pT180/pY182) immunoreactivity around the needle track when the IL-1Ra was included with microglia from 6-month-old hTau*Cx3cr1*$^{-/-}$ donor mice (**B**) compared to those receiving hTau*Cx3cr1*$^{-/-}$ donor microglia alone (**A**). Scale bar = 30 μm. Quantification of percentage p-p38 MAPK immunoreactive area revealed a statistically significant (*$P < 0.05$; $n = 3$ animals per group; three sections per mice and four fields per section were used; mean ± SEM; unpaired *t*-test) decrease in the p-p38 MAPK^{+} area in the brains of non-transgenic mice that receiving microglia from hTau*Cx3cr1*$^{-/-}$ donor mice (**E**). (**C** and **D**) Triple immunofluorescence analysis revealing EGFP^{+} donor microglia within the recipient mouse brain. The area surrounding such microglia display relatively less p-p38 MAPK immunoreactivity (red in **D**) when the IL-1Ra was included with hTau*Cx3cr1*$^{-/-}$microglial inoculum. Scale bar = 20 μm.

Discussion

In the current study we demonstrate that genetically enhancing microglia-specific neuroinflammation significantly accelerates the onset and progression of tau pathology, cognitive dysfunction and neurodegeneration in hTau *Cx3cr1*$^{-/-}$ mice. Second, we observe that microglial activation may contribute to the spread of tau pathology through anatomically connected neurons of the hippocampus. Finally, adoptive transfer of microglia from hTau*Cx3cr1*$^{-/-}$ mice can induce hyperphosphorylation of endogenous mouse tau within the recipient mice brains.

We performed an age-based study to assess the effect of microglial neuroinflammation in 2-, 6-, 12- and 24-month old hTau*Cx3cr1*$^{-/-}$ mice. Intriguingly, this corresponds to 7-, 16-, 33- and 65-years of age in humans (Demetrius, 2006). Evidence of increased neuroinflammation leading to tau pathology is relevant because of the occurrence of brain inflammation often observed in children and young adults following CNS infections with the likelihood of cognitive problems in areas of executive function and working memory. For example, children affected with encephalitis have been observed to display problems with anxiety, executive and cognitive function (Fowler *et al.*, 2013). Similarly, memory impairment is often encountered as a result of closed head injury and/or resulting inflammatory responses in younger children (Capruso and Levin, 1992) involved in contact sports (reviewed in McKee *et al.*, 2013). Therefore, the current study provides a basis for some of these human conditions with enhanced brain inflammation, which eventually lead to impairments in a number of cognitive domains.

Several previous studies have suggested that neuroinflammation precedes tau pathology and leads to cognitive impairment in chronic neurodegenerative mouse models such as Alzheimer's disease. First, induction of systemic inflammation with lipopolysaccharide (Kitazawa *et al.*, 2005) or PolyI:C (Krstic *et al.*, 2012) in young or pre-natal 3xTg mouse model of Alzheimer's disease, respectively, resulted in enhanced microglial activation and tau pathology. Second, microglial activation preceded tau pathology and synaptic loss in the P301S mouse model of tauopathy (Yoshiyama *et al.*, 2007). Notably, in the same study administration of FK506, an anti-inflammatory compound, not only reduced tau pathology, it also prolonged the lifespan of P301S mice. Finally, in our previous study, deficiency of CX3CR1 in hTau mice resulted in tau hyperphosphorylation and aggregation as well as impaired

working memory at 6 months of age (Bhaskar *et al.*, 2010). These studies suggest that microglial activation and brain inflammation may worsen the disease by exacerbating tau pathology. Appearance of hyperphosphorylated tau, maturation of IL1B, activation of Iba1$^+$ microglia and increased CD68 expression in hTau*Cx3cr1*$^{-/-}$ mice as early as 2 months of age in the present study also supported this possibility.

As microglia-mediated neuroinflammation seems to be an early event in the progression of the disease, and manipulation of inflammatory pathways changes the course of the disease, it is very likely that once the inflammatory alterations have begun, they lead to a feed-forward activation of disease-related pathways (Wyss-Coray, 2006). In support of this, recent evidence suggests that there are altered inflammatory components in Alzheimer's disease. First, inflammatory cells (microglia and astrocytes), cytokines, chemokines, and complement components are elevated in Alzheimer's disease compared to control brains (McGeer and McGeer, 2001). Second, these inflammatory changes occur before the deposition of amyloid-β (Dudal *et al.*, 2004; Kitazawa *et al.*, 2005) and pathological aggregation of tau (Yoshiyama *et al.*, 2007) in several different mouse models of Alzheimer's disease. Third, patients receiving sustained treatment with non-steroidal anti-inflammatory drugs (NSAIDs) during mid-life exhibited a $>50\%$ decreased risk of Alzheimer's disease in retrospective studies (McGeer *et al.*, 1996). Although prospective studies with NSAIDs have been unsuccessful—reviewed in McGeer and McGeer (2007)—this may reflect that NSAIDs offer pre-morbid, but not therapeutic protection. Fourth, a recent genome-wide association study (GWAS) identified a single-nucleotide polymorphism within the CR1 locus, encoding the complement component (3b/4b) on chromosome 1, to be associated with sporadic Alzheimer's disease (Lambert *et al.*, 2009). Notably, *CD33* and *MS4A4/MS4A6E*, genes related to the regulation of the immune system, have been shown to have a significant association with sporadic Alzheimer's disease (Hollingworth *et al.*, 2011; Naj *et al.*, 2011). Finally, an arginine-to-histidine substitution at amino acid 47 (R47H) in the triggering receptor expressed on myeloid cells 2 (*TREM2*) gene, which regulates microglial function in the CNS, increased the risk of developing late-onset Alzheimer's disease by 3-fold (Guerreiro *et al.*, 2013; Jonsson *et al.*, 2013). Collectively, these studies suggest that inflammatory pathways directly contribute to the development and progression of Alzheimer's disease.

An initial increase (at 2 months of age) and subsequent decrease (at 12 and 24 months of age) in the levels of AT8, AT180 and PHF-1 positive tau in hTau*Cx3cr1*$^{-/-}$ mice may be attributed to the onset of neuronal loss in hTau mice around 12–14 months of age (Andorfer *et al.*, 2005). Furthermore, modest reduction in the number of phosphorylated tau positive neurons was evident in the immunohistochemical analysis. In support of this possibility, the CA1 layer appeared thinner as early as 2 months of age, a significant reduction in the NeuN$^+$ cells at 12 months of age and reduced hippocampal weight at 24 months of age in hTau*Cx3cr1*$^{-/-}$ mice.

An interesting pattern of activation of p38 MAPK was observed during the course of disease in hTau*Cx3cr1*$^{-/-}$ mice. First, p38 MAPK was initially activated in hTau and hTau*Cx3cr1*$^{-/-}$ mice at 2 months of age and then it was reduced at 6 months of age. A secondary phase of activation was observed between 12 and 24 months of age. Age-related alterations in the activation of p38 MAPK have been previously described (Zhen *et al.*, 1999). Second, p38 MAPK has been demonstrated to be a cytokine inducer (Lee *et al.*, 1994), an important regulator of embryonic development and cancer (Bradham and McClay, 2006) as well as neurogenesis (Sato *et al.*, 2008). Finally, p38 MAPK has been shown to phosphorylate tau in several mouse models of tauopathy (Li *et al.*, 2003; Lambourne *et al.*, 2005; Kelleher *et al.*, 2007; Bhaskar *et al.*, 2010). While the active p38 MAPK levels correlate with early-stage tau phosphorylation in hTau*Cx3cr1*$^{-/-}$ mice at 2 months of age, further studies are necessary to differentiate developmental versus disease-specific activation of p38 MAPK at these early ages.

Adding to the complexity is the CX3CL1-CX3CR1 signalling within the CNS, which is a complex and highly regulated process (Ransohoff and Cardona, 2010; Reaux-Le Goazigo *et al.*, 2013). This is further complicated by the type and severity of the insult causing damage to the CNS (Sheridan and Murphy, 2013). For example, many studies have suggested CX3CR1 deficiency exacerbates the pathology (Cho *et al.*, 2011), whereas other studies suggest that CX3CR1 deficiency is protective (Denes *et al.*, 2008). Notably, two previous studies have documented opposite effects on synaptic and cognitive function in CX3CR1 deficient mice (Maggi *et al.*, 2011; Rogers *et al.*, 2011). In Rogers *et al.* (2011), the gene dose effect of CX3CR1 deficiency on memory impairment was linked to the elevated levels of IL1B. Blocking IL1b signalling via IL-1Ra treatment in *Cx3cr1*$^{-/-}$ hippocampal slices restored long-term potentiation. Similarly infusing IL-1Ra into the ventricles of live *Cx3cr1*$^{-/-}$ mice rescued hippocampal-dependent learning (Rogers *et al.*, 2011). On the other hand, Maggi *et al.* (2011) observed increased hippocampal plasticity and spatial memory in *Cx3cr1*$^{-/-}$ mice. While these two studies are contradictory, they suggest the complexity of CX3CL1-CX3CR1 signalling due to gender and hormonal systems, as only males were used in Rogers *et al.* (2011) and only females were used in Maggi *et al.* (2011) studies. In contrast to these two studies, we used mice with mixed gender and observed a significant delay in finding the hidden platform on different days for hTau and hTau*Cx3cr1*$^{-/-}$ mice when we performed day-wise comparisons with non-transgenic mice (Fig. 3E). This would suggest a possible impairment in retention or consolidation of spatial memory at 6 months of age. However, at 12-months of age, only hTau*Cx3cr1*$^{-/-}$ mice showed significant impairment in

the probe test compared to age-matched non-transgenic mice (Fig. 3F–H).

Our results from adoptive transfer studies have suggested that microglia derived from the highly pro-inflammatory milieu of the hTau*Cx3cr1*$^{-/-}$ mouse brain are sufficient to induce AT8 site phosphorylation and a 'pre-tangle-type' aggregation of endogenous mouse tau within the recipient mouse brain. In a previous study, we used a similar strategy to demonstrate that microglia derived from lipopolysaccharide-administered *Cx3cr1*$^{-/-}$ mice was capable of inducing apoptosis within the recipient mouse brain (Cardona *et al.*, 2006). Notably, adoptive transfer of *Cx3cr1*$^{-/-}$ microglia into the brains of *Il1r1*$^{-/-}$ mice did not cause neurotoxicity, suggesting that this microglial-specific effect is mediated via the IL-1R pathway. Several previous studies have implicated the IL1B–p38 MAPK pathway in inducing tau pathology. First, a polymorphism in the *IL1B* gene is associated with human Alzheimer's disease (Di Bona *et al.*, 2008; Payao *et al.*, 2012; Yuan *et al.*, 2013; Flex *et al.*, 2014). Second, impregnation of IL1B pellets within the rat brain significantly increased the levels of p38 MAPK and tau phosphorylation (Sheng *et al.*, 2001). Third, numerous studies have documented an overstimulation of TLR/IL-1R/IL-1R-associated kinases/NF-κB signalling pathway present within the brains of different tauopathies (Colangelo *et al.*, 2002; Lukiw, 2004; Cui *et al.*, 2007). Fourth, enhancing or blocking IL1B expression exacerbates (Ghosh *et al.*, 2013) or inhibits (Kitazawa *et al.*, 2011) tau pathology, respectively, and the latter rescues cognition in 3xTg-Alzheimer's disease mice (Kitazawa *et al.*, 2011). Finally, our previous study demonstrated that microglial neuroinflammation exacerbates tau pathology in part mediated via activation of the neuronal IL-1R–p38 MAPK pathway (Bhaskar *et al.*, 2010). These studies, together with the results from the present study, suggest that IL1B secreted from activated microglia is sufficient to drive tau pathology within the naïve mouse brain.

Finally, our data suggest that alterations in microglial morphology may prime the brain microenvironment that is destined to participate in the propagation of misfolded tau within the anatomically connected regions of the brain. It is still unclear whether microglia will be involved in the uptake and transfer of tau proteins between neurons. It is conceivable to expect this may be true based on recent studies, which suggest that misprocessed tau may be released from neurons via exosomes (Saman *et al.*, 2012), which would most likely be taken up by microglial cells. Clear co-localization of AT8^{+} tau with Iba1^{+} microglia has also been observed in a rodent model of tauopathy (Zilka *et al.*, 2012).

In conclusion, this study provides a comprehensive view on the progression of tau pathology in response to genetic induction of brain inflammation in a mouse model of tauopathy. Our study also suggests that reactive microglia are sufficient to promote tau pathology in a cell-autonomous manner. Future therapeutic strategies targeting CX3CL1-CX3CR1 and/or IL1B signalling will be beneficial against the pathological progression of tau pathology.

Supplementary material

Supplemental material is available at *Brain* online.

Acknowledgements

We thank Megan Konerth for initial adoptive transfer and behavioural studies. Dr Steve Stohlman and Dr Timothy Pharres for assisting us with the microglial isolation, Dr Susan Staugaitis for providing human Alzheimer's disease brain tissue and Dr Vojo Deretic for sharing HEK-Blue^{TM} IL1B cells. Dr Bryce Chackerian for reading the manuscript and for comments. We thank UNM Cancer Centre Microscopy Core Facility for their assistance in generating high quality images and quantitative morphometric analysis.

Funding

This work was supported by CurePSP (#472-09), UNM CoBRE P30 Pilot and UNM SOM RAC Awards, Alzheimer's Association (NIRG-11-204995) and NIH/NINDS (R21NS077089 and R01NS083704) funding to K.B. Alzheimer's Association (MCPG to B.T.L and R.M.R) and Bright Focus Foundation Pilot Award (AHAF0311KB to K.B/B.T.L), DOD (ERMS#12109018 to B.T.L) and NIH (AG023012 to B.T.L; NS074804 to B.T.L and R.M.R; GM095426-02 to A.C.).

References

Andorfer C, Acker CM, Kress Y, Hof PR, Duff K, Davies P. Cell-cycle reentry and cell death in transgenic mice expressing nonmutant human tau isoforms. J Neurosci 2005; 25: 5446–54.

Andorfer C, Kress Y, Espinoza M, de Silva R, Tucker KL, Barde YA, et al. Hyperphosphorylation and aggregation of tau in mice expressing normal human tau isoforms. J Neurochem. 2003; 86: 582–90.

Bhaskar K, Maphis N, Xu G, Varvel NH, Kokiko-Cochran ON, Weick JP, et al. Microglial derived tumor necrosis factor-alpha drives Alzheimer's disease-related neuronal cell cycle events. Neurobiol Dis 2014; 62: 273–85.

Bhaskar KaL, B.T. The role of Aβ and tau oligomers in the pathogenesis of Alzheimer's disease. In: Rahimi FaB G, editor. Non-fibrillar amyloidogenic protein assemblies—common cytotoxins underlying degenerative diseases. New York: Springer Science + Business Media B.V. 2012, p. 135–88.

Bhaskar K, Konerth M, Kokiko-Cochran ON, Cardona A, Ransohoff RM, Lamb BT. Regulation of tau pathology by the microglial fractalkine receptor. Neuron 2010; 68: 19–31.

Bellucci A, Bugiani O, Ghetti B, Spillantini MG. Presence of reactive microglia and neuroinflammatory mediators in a case of frontotemporal dementia with P301S mutation. Neurodegener Dis 2011; 8: 221–9.

Bellucci A, Westwood AJ, Ingram E, Casamenti F, Goedert M, Spillantini MG. Induction of inflammatory mediators and microglial

activation in mice transgenic for mutant human P301S tau protein. Am J Pathol 2004; 165: 1643–52.
Bergmann CC, Yao Q, Stohlman SA. Microglia exhibit clonal variability in eliciting cytotoxic T lymphocyte responses independent of class I expression. Cell Immunol 1999; 198: 44–53.
Burns K, Martinon F, Tschopp J. New insights into the mechanism of IL-1beta maturation. Curr Opin Immunol 2003; 15: 26–30.
Braak H, Braak E. Demonstration of amyloid deposits and neurofibrillary changes in whole brain sections. Brain Pathol 1991; 1: 213–6.
Bradham C, McClay DR. p38 MAPK in development and cancer. Cell Cycle 2006; 5: 824–8.
Cardona AE, Pioro EP, Sasse ME, Kostenko V, Cardona SM, Dijkstra IM, et al. Control of microglial neurotoxicity by the fractalkine receptor. Nat Neurosci 2006; 9: 917–24.
Capruso DX, Levin HS. Cognitive impairment following closed head injury. Neurol Clin 1992; 10: 879–93.
Cho SH, Sun B, Zhou Y, Kauppinen TM, Halabisky B, Wes P, et al. CX3CR1 protein signaling modulates microglial activation and protects against plaque-independent cognitive deficits in a mouse model of Alzheimer disease. J Biol Chem 2011; 286: 32713–22.
Clark SR, McMahon CJ, Gueorguieva I, Rowland M, Scarth S, Georgiou R, et al. Interleukin-1 receptor antagonist penetrates human brain at experimentally therapeutic concentrations. J Cereb Blood Flow Metab 2008; 28: 387–94.
Colangelo V, Schurr J, Ball MJ, Pelaez RP, Bazan NG, Lukiw WJ. Gene expression profiling of 12633 genes in Alzheimer hippocampal CA1: transcription and neurotrophic factor down-regulation and up-regulation of apoptotic and pro-inflammatory signaling. J Neurosci Res 2002; 70: 462–73.
Cui JG, Hill JM, Zhao Y, Lukiw WJ. Expression of inflammatory genes in the primary visual cortex of late-stage Alzheimer's disease. Neuroreport 2007; 18: 115–9.
Demetrius L. Aging in mouse and human systems: a comparative study. Ann N Y Acad Sci 2006; 1067: 66–82.
Denes A, Ferenczi S, Halasz J, Kornyei Z, Kovacs KJ. Role of CX3CR1 (fractalkine receptor) in brain damage and inflammation induced by focal cerebral ischemia in mouse. J Cereb Blood Flow Metab 2008; 28: 1707–21.
Di Bona D, Plaia A, Vasto S, Cavallone L, Lescai F, Franceschi C, et al. Association between the interleukin-1beta polymorphisms and Alzheimer's disease: a systematic review and meta-analysis. Brain Res Rev 2008; 59: 155–63.
Dudal S, Krzywkowski P, Paquette J, Morissette C, Lacombe D, Tremblay P, et al. Inflammation occurs early during the Abeta deposition process in TgCRND8 mice. Neurobiol Aging 2004; 25: 861–71.
Flex A, Giovannini S, Biscetti F, Liperoti R, Spalletta G, Straface G, et al. Effect of proinflammatory gene polymorphisms on the risk of Alzheimer's disease. Neurodegener Dis 2014; 13: 230–6.
Fowler A, Forsman L, Eriksson M, Wickstrom R. Tick-borne encephalitis carries a high risk of incomplete recovery in children. J Pediatrics 2013; 163: 555–60.
Frost B, Jacks RL, Diamond MI. Propagation of tau misfolding from the outside to the inside of a cell. J Biol Chem 2009; 284: 12845–52.
Gallagher M, Burwell R, Burchinal M. Severity of spatial learning impairment in aging: development of a learning index for performance in the Morris Water Maze. Behav Neurosci 1993; 107: 618–26.
Gebicke-Haerter PJ. Microglia in neurodegeneration: molecular aspects. Microsc Res Tech 2001; 54: 47–58.
Gerhard A, Trender-Gerhard I, Turkheimer F, Quinn NP, Bhatia KP, Brooks DJ. *In vivo* imaging of microglial activation with [11C](R)-PK11195 PET in progressive supranuclear palsy. Mov Disord 2006; 21: 89–93.
Gerhard A, Watts J, Trender-Gerhard I, Turkheimer F, Banati RB, Bhatia K, et al. *In vivo* imaging of microglial activation with [11C](R)-PK11195 PET in corticobasal degeneration. Mov Disord 2004; 19: 1221–6.
Ghosh S, Wu MD, Shaftel SS, Kyrkanides S, Laferla FM, Olschowka JA, et al. Sustained interleukin-1beta overexpression exacerbates tau pathology despite reduced amyloid burden in an Alzheimer's mouse model. J Neurosci 2013; 33: 5053–64.
Guerreiro R, Wojtas A, Bras J, Carrasquillo M, Rogaeva E, Majounie E, et al. TREM2 variants in Alzheimer's disease. N Engl J Med 2013; 368: 117–27.
Greenberg SG, Davies P. A preparation of Alzheimer paired helical filaments that displays distinct tau proteins by polyacrylamide gel electrophoresis. Proc Natl Acad Sci USA 1990; 87: 5827–31.
Ho GJ, Drego R, Hakimian E, Masliah E. Mechanisms of cell signaling and inflammation in Alzheimer's disease. Curr Drug Targets Inflamm Allergy 2005; 4: 247–56.
Hollingworth P, Harold D, Sims R, Gerrish A, Lambert JC, Carrasquillo MM, et al. Common variants at ABCA7, MS4A6A/MS4A4E, EPHA1, CD33 and CD2AP are associated with Alzheimer's disease. Nat Genet 2011; 43: 429–35.
Ikeda M, Shoji M, Kawarai T, Kawarabayashi T, Matsubara E, Murakami T, et al. Accumulation of filamentous tau in the cerebral cortex of human tau R406W transgenic mice. Am J Pathol 2005; 166: 521–31.
Ishizawa K, Dickson DW. Microglial activation parallels system degeneration in progressive supranuclear palsy and corticobasal degeneration. J Neuropathol Exp Neurol 2001; 60: 647–57.
Jonsson T, Stefansson H, Steinberg S, Jonsdottir I, Jonsson PV, Snaedal J, et al. Variant of TREM2 associated with the risk of Alzheimer's disease. N Engl J Med 2013; 368: 107–16.
Jung S, Aliberti J, Graemmel P, Sunshine MJ, Kreutzberg GW, Sher A, et al. Analysis of fractalkine receptor CX(3)CR1 function by targeted deletion and green fluorescent protein reporter gene insertion. Mol Cell Biol 2000; 20: 4106–14.
Kelleher I, Garwood C, Hanger DP, Anderton BH, Noble W. Kinase activities increase during the development of tauopathy in htau mice. J Neurochem 2007; 103: 2256–67.
Kitazawa M, Oddo S, Yamasaki TR, Green KN, LaFerla FM. Lipopolysaccharide-induced inflammation exacerbates tau pathology by a cyclin-dependent kinase 5-mediated pathway in a transgenic model of Alzheimer's disease. J Neurosci 2005; 25: 8843–53.
Kitazawa M, Cheng D, Tsukamoto MR, Koike MA, Wes PD, Vasilevko V, et al. Blocking IL-1 signaling rescues cognition, attenuates tau pathology, and restores neuronal beta-catenin pathway function in an Alzheimer's disease model. J Immunol 2011; 187: 6539–49.
Krstic D, Madhusudan A, Doehner J, Vogel P, Notter T, Imhof C, et al. Systemic immune challenges trigger and drive Alzheimer-like neuropathology in mice. J Neuroinflam 2012; 9: 151.
Lambert JC, Heath S, Even G, Campion D, Sleegers K, Hiltunen M, et al. Genome-wide association study identifies variants at CLU and CR1 associated with Alzheimer's disease. Nat Genet 2009; 41: 1094–9.
Lambourne SL, Sellers LA, Bush TG, Choudhury SK, Emson PC, Suh YH, et al. Increased tau phosphorylation on mitogen-activated protein kinase consensus sites and cognitive decline in transgenic models for Alzheimer's disease and FTDP-17: evidence for distinct molecular processes underlying tau abnormalities. Mol Cell Biol 2005; 25: 278–93.
Lamkanfi M, Dixit VM. The inflammasomes. PLoS Pathog 2009; 5: e1000510.
Lee JC, Laydon JT, McDonnell PC, Gallagher TF, Kumar S, Green D, et al. A protein kinase involved in the regulation of inflammatory cytokine biosynthesis. Nature 1994; 372: 739–46.
Lee VM, Goedert M, Trojanowski JQ. Neurodegenerative tauopathies. Annu Rev Neurosci 2001; 24: 1121–59.
Li Y, Liu L, Barger SW, Griffin WS. Interleukin-1 mediates pathological effects of microglia on tau phosphorylation and on

synaptophysin synthesis in cortical neurons through a p38-MAPK pathway. J Neurosci 2003; 23: 1605–11.
Liu L, Drouet V, Wu JW, Witter MP, Small SA, Clelland C, et al. Trans-synaptic spread of tau pathology *in vivo*. PloS One 2012; 7: e31302.
Lukiw WJ. Gene expression profiling in fetal, aged, and Alzheimer hippocampus: a continuum of stress-related signaling. Neurochem Res 2004; 29: 1287–97.
Maei HR, Zaslavsky K, Teixeira CM, Frankland PW. What is the most sensitive measure of Water Maze probe test performance? Front Integr Neurosci 2009; 3: 4.
Maggi L, Scianni M, Branchi I, D'Andrea I, Lauro C, Limatola C. CX(3)CR1 deficiency alters hippocampal-dependent plasticity phenomena blunting the effects of enriched environment. Front Cell Neurosci 2011; 5: 22.
McGeer PL, McGeer EG. Inflammation, autotoxicity and Alzheimer disease. Neurobiol Aging 2001; 22: 799–809.
McGeer PL, McGeer EG. NSAIDs and Alzheimer disease: epidemiological, animal model and clinical studies. Neurobiol Aging 2007; 28: 639–47.
McGeer PL, Schulzer M, McGeer EG. Arthritis and anti-inflammatory agents as possible protective factors for Alzheimer's disease: a review of 17 epidemiologic studies. Neurology 1996; 47: 425–32.
McKee AC, Stein TD, Nowinski CJ, Stern RA, Daneshvar DH, Alvarez VE, et al. The spectrum of disease in chronic traumatic encephalopathy. Brain 2013; 136(Pt 1): 43–64.
Morris M, Maeda S, Vossel K, Mucke L. The many faces of tau. Neuron 2011; 70: 410–26.
Morris R. Developments of a water-maze procedure for studying spatial learning in the rat. J Neurosci Methods 1984; 11: 47–60.
Naj AC, Jun G, Beecham GW, Wang LS, Vardarajan BN, Buros J, et al. Common variants at MS4A4/MS4A6E, CD2AP, CD33 and EPHA1 are associated with late-onset Alzheimer's disease. Nat Genet 2011; 43: 436–41.
Payao SL, Goncalves GM, de Labio RW, Horiguchi L, Mizumoto I, Rasmussen LT, et al. Association of interleukin 1beta polymorphisms and haplotypes with Alzheimer's disease. J Neuroimmunol 2012; 247: 59–62.
Ransohoff RM, Cardona AE. The myeloid cells of the central nervous system parenchyma. Nature 2010; 468: 253–62.
Reaux-Le Goazigo A, Van Steenwinckel J, Rostene W, Melik Parsadaniantz S. Current status of chemokines in the adult CNS. Prog Neurobiol 2013; 104: 67–92.
Rogers JT, Morganti JM, Bachstetter AD, Hudson CE, Peters MM, Grimmig BA, et al. CX3CR1 deficiency leads to impairment of hippocampal cognitive function and synaptic plasticity. J Neurosci 2011; 31: 16241–50.
Saman S, Kim W, Raya M, Visnick Y, Miro S, Saman S, et al. Exosome-associated tau is secreted in tauopathy models and is selectively phosphorylated in cerebrospinal fluid in early Alzheimer disease. J Biol Chem 2012; 287: 3842–9.
Sato K, Hamanoue M, Takamatsu K. Inhibitors of p38 mitogen-activated protein kinase enhance proliferation of mouse neural stem cells. J Neurosci Res 2008; 86: 2179–89.
Saura J, Tusell JM, Serratosa J. High-yield isolation of murine microglia by mild trypsinization. Glia 2003; 44: 183–9.
Sasaki A, Kawarabayashi T, Murakami T, Matsubara E, Ikeda M, Hagiwara H, et al. Microglial activation in brain lesions with tau deposits: comparison of human tauopathies and tau transgenic mice TgTauP301L. Brain Res 2008; 1214: 159–68.
Sheng JG, Jones RA, Zhou XQ, McGinness JM, Van Eldik LJ, Mrak RE, et al. Interleukin-1 promotion of MAPK-p38 overexpression in experimental animals and in Alzheimer's disease: potential significance for tau protein phosphorylation. Neurochem Int 2001; 39: 341–8.
Sheridan GK, Murphy KJ. Neuron-glia crosstalk in health and disease: fractalkine and CX3CR1 take centre stage. Open Biol 2013; 3: 130181.
Wyss-Coray T. Inflammation in Alzheimer disease: driving force, bystander or beneficial response? Nat Med 2006; 12: 1005–15.
Yoshiyama Y, Higuchi M, Zhang B, Huang SM, Iwata N, Saido TC, et al. Synapse loss and microglial activation precede tangles in a P301S tauopathy mouse model. Neuron 2007; 53: 337–51.
Yuan H, Xia Q, Ge P, Wu S. Genetic polymorphism of interleukin 1beta -511C/T and susceptibility to sporadic Alzheimer's disease: a meta-analysis. Mol Biol Reports 2013; 40: 1827–34.
Zhen X, Uryu K, Cai G, Johnson GP, Friedman E. Age-associated impairment in brain MAPK signal pathways and the effect of caloric restriction in Fischer 344 rats. J Gerontol A Biol Sci Med Sci 1999; 54: B539–48.
Zilka N, Kazmerova Z, Jadhav S, Neradil P, Madari A, Obetkova D, et al. Who fans the flames of Alzheimer's disease brains? Misfolded tau on the crossroad of neurodegenerative and inflammatory pathways. J Neuroinflamm 2012; 9: 47.
Zilka N, Stozicka Z, Kovac A, Pilipcinec E, Bugos O, Novak M. Human misfolded truncated tau protein promotes activation of microglia and leukocyte infiltration in the transgenic rat model of tauopathy. J Neuroimmunol 2009; 209: 16–25.